Available online at www.sciencedirect.com
SCIENCE DIRECT®
Gene 356 (2005) 39 – 48
GENE
SECTION
FUNCTIONAL GENOMICS
www.elsevier.com/locate/gene

Influence of inhalation anesthesia assessed by comprehensive gene expression profiling☆

Atsuhiro Sakamoto[a,*], Jun-ichi Imai[b,c], Akira Nishikawa[c,d], Reiko Honma[b], Emi Ito[b], Yuka Yanagisawa[b], Mika Kawamura[c], Ryo Ogawa[a], Shinya Watanabe[b,*]

[a]*Department of Anesthesiology, Nippon Medical School, Sendagi, Bunkyo-ku, Tokyo 113-8603, Japan*
[b]*Department of Clinical Informatics, Tokyo Medical and Dental University, Yushima, Bunkyo-ku, Tokyo 113-8519, Japan*
[c]*Medicrome, Inc., Sendagaya, Shibuya-ku, Tokyo 151-0051, Japan*
[d]*Nippon Gene, Co., Ltd, Kandanishiki-cho, Chiyoda-ku, Tokyo 101-0054, Japan*

Received 15 October 2004; received in revised form 14 February 2005; accepted 1 March 2005
Available online 20 June 2005
Received by T. Gojobori

Abstract

Although general anesthesia is routinely used as an essential surgical procedure and its harmlessness has been evaluated and endorsed by clinical outcomes, little is known about its comprehensive influence that is not reflected in mortality and morbidity. In this paper, we have shown that inhalation anesthesia affected the expression of < 1.5% of > 10,000 genes, by analyzing the expression profiles for multiple organs of rats anesthetized with sevoflurane. The small number of transcripts affected by the inhalation anesthesia comprised those specific to single and common in multiple organs. The former included genes mainly associated with drug metabolism in the liver and influenced by agents such as amphetamine in the brain. The latter contained multiple circadian genes. In the brain, we failed to detect the alteration of the clock gene expression with the exception of *Per2*, assuming that anesthesia perturbs circadian rhythms. Our findings provide the first assessment for the influence of inhalation anesthesia by approaches of experimental biology and genome science.

Keywords: General anesthesia; Gene expression profile; DNA microarray; Circadian gene; Endothelin1; *Per2*

1. Introduction

Inhalation anesthetics induce general anesthesia that results in unconsciousness, insensitivity to pain, and lack of memory of pain. Although general anesthesia has been routinely used as an essential surgical procedure for approximately 150 years and its harmlessness has been evaluated and endorsed by clinical outcomes (Forrest et al., 1990; Levy, 1984; Brown and Frink, 1993), little is known with regard to its comprehensive influence, which is not reflected in mortality and morbidity. A few studies were reported on the results of inhalation anesthesia on cells and tissues at the molecular level. This anesthetic acted upon an extremely restricted number of genes including those that control the expression of ligand-gated ion channels and G-protein-coupled receptors (Franks and Lieb, 1994; Harris et al., 1995).

The recent progress in genomics enables us to comprehensively describe and analyze the alteration in cells and tissues at the gene expression level by hybridization with DNA microarrays representing genome-wide or subgenome-wide species of transcripts. Therefore, we attempted to comprehensively analyze the effects of

Abbreviations: Arc, activity-regulated cytoskeleton; Bmal1, Brain-Muscle-Arnt-Like-protein 1; Cry2, Cryptochrome2; Dbp, albumin site d-binding protein; Egr1, early growth response gene-1; NGFI-B, nerve growth factor-induced gene B; PCR, polymerase chain reaction; Per2, Period2; SD, standard deviation; Tef, thyrotroph embryonic factor.

☆ Data from all the arrays used in this paper will be available at DDBJ via CIBEX (http://www.cibex.nig.ac.jp/cibex/HTML/index.html) under accession nos.: for the array design, CBX4; for the experiments, CAR4.

* Corresponding authors. Tel.: +81 3 5414 6010; fax: +81 3 5775 1352.
E-mail addresses: no1-saka@nms.ac.jp (A. Sakamoto)
swata@mvc.biglobe.ne.jp (S. Watanabe).

0378-1119/$ - see front matter © 2005 Elsevier B.V. All rights reserved.
doi:10.1016/j.gene.2005.03.022

inhalation anesthesia at the molecular level by obtaining gene expression profiles from rats under inhalation anesthesia.

In this study, we have shown that inhalation anesthesia affected expression of an extremely limited number of genes. This was done by analyzing expression profiles for multiple organs of rats at different time points after anesthetizing with sevoflurane. Our findings could provide a basis for exploring comprehensive influence of inhalation anesthesia and to endorse the safety of anesthesia in the future. The expression profiling analyses also demonstrate the possible association between the anesthetic status and alteration in modulation of the circadian gene expression that were previously identified in addition to nominating novel candidates for the circadian gene.

2. Materials and methods

2.1. Animals and tissue collection

Six-week-old male rats (Wister; Charles River Japan, Inc., Atsugi, Japan) were purchased and adapted to a 12-h light/12-h dark cycle starting at 06:00 and 18:00 for a week before the experiments. The anesthesia experiment was replicated twice with an interval of several weeks between the two experiments (Exp. 1 and Exp. 2). Anesthesia was used at 09:00 on nine rats in Exp. 1 and on 10 rats in Exp. 2. Rats were housed in a plastic box supplied with sevoflurane (4.5% air mixture gas) at the rate of 6 L/min. As the 0-h control, rats ($n=3$, in Exp. 1; $n=4$, in Exp. 2) were subjected to tracheal intubation immediately after induction of anesthesia in order to maintain the anesthetic status and sacrificed to obtain organs. The organs were obtained in the order of the blood, the spleen, the kidneys, the liver, the lungs, the heart, and the brain within 5–10 min per animal after the intubation. As the 2-h and 6-h samples, the anesthetized rats were picked up from the plastic box supplied with sevoflurane, subjected to the intubation, and sacrificed to similarly obtain the organs 2 h and 6 h after induction of anesthesia, respectively. Three rats were used for each time point of each experiment with the exception of the time point of 0 h in Exp. 2, in which four rats were used; eventually, a total of 19 rats were used in the two replicated experiments.

2.2. RNA preparation

The blood obtained was immediately mixed with an ISOGEN-LS reagent (NIPPON GENE, Tokyo, Japan) after dilution with an equal volume of water. The other organs (the whole brain, the whole heart, the left lung, the lateral left lobe of the liver, the whole spleen, and both the kidneys) were immediately frozen in liquid nitrogen and lysed with an ISOGEN reagent (NIPPON GENE). Total RNA was prepared from the lysate in accordance with the manufacturer's instructions. Poly(A)+ RNA was prepared from total RNA with a Poly(A) Purist Kit (Ambion, TX, USA), in accordance with the manufacturer's instructions.

2.3. Microarray preparation and expression profile acquisition

A set of synthetic polynucleotides (80-mers) that represented 11,464 rat transcripts derived from 10,490 independent genes, including most of the RefSeq clones deposited in the NCBI database (MicroDiagnostic, Tokyo, Japan), was arrayed on a slide glass (S9115; Matsunami, Kishiwada, Japan) with a custom-made arrayer (Kobayashi et al., 2004; Ito et al., 2003). Poly(A)+ RNA (2 μg) was labeled with SuperScript II (Invitrogen, CA, USA) and Cyanine 5-dUTP for each sample or Cyanine 3-dUTP (PerkinElmer, MA, USA) for a rat common reference RNA (MicroDiagnostic). Labeling, hybridization, and subsequent washes of microarrays were performed with a Labeling and Hybridization Kit (MicroDiagnostic), in accordance with the manufacturer's instructions. The rat common reference RNA was purchased as a single batch and labeled as an aliquot with Cyanine-3 for a single microarray side by side with each sample which was labeled with Cyanine-5. Hybridization signals were measured using a GenePix 400A scanner (Axon Instruments, CA, USA) and then processed into primary expression ratios ([Cyanine 5-intensity obtained from each sample]/[Cyanine 3-intensity obtained from the rat common reference RNA], which are indicated as 'median of ratios' in GenePix Pro 3.0 software (Axon Instruments)). Normalization was performed for the median of ratios (primary expression ratios) by multiplying normalization factors calculated for each feature on a microarray by the GenePix Pro 3.0 software. All the data in accordance with the MIAME guideline were deposited at DDBJ via CIBEX (http://www.cibex.nig.ac.jp/cibex/HTML/index.html) under accession numbers CBX4 (for the array design) and CAR4 (for the experiments).

2.4. Data analysis

Data processing and subsequent hierarchical clustering analysis were performed with an Excel program (Microsoft, WA, USA) and an MDI gene expression analysis software package (MicroDiagnostic). The primary expression ratios were converted into $\log_2$ values ($\log_2$ Cyanine-5 intensity/Cyanine-3 intensity) (designated log ratios) and compiled into a matrix (designated primary data matrix).

We conducted the following operations to extract genes, from the primary data matrix, in which the expression levels altered specifically on inhalation anesthesia. (i) The mean average of log ratios for each 0-h data set of each organ (designated 0-h averages) was calculated. (ii) The relative ratios against the respective 0-h average values for all the log ratios (designated relative log ratios) were generated. This enabled us to compare all data as expression differences that deviated from the mean average

of each gene and to introduce a single threshold value (=0.75) to filter the genes in which the expression levels altered. (iii) All the relative log ratios were arranged into a matrix (designated secondary data matrix). (iv) In order to filter out the genes in which the expression levels deviated from the mean average in an individual data set for each gene, each time point, and each organ, we calculated standard deviation of relative log ratios for each time point and each organ, using the data from all the animals (Exp. 1 and Exp. 2). The SD values calculated by every organ showed similar distributions and there was no obvious correlation between the SD values and the fluorescent intensities initially detected in each microarray. This enabled us to introduce a single SD value (=1.0) as a cutoff threshold for all the genes. The calculated value should reflect the differences between independently repeated anesthetic experiments and the responses of individual rats. (v) The genes with standard deviation of the relative log ratios greater than 1 for at least one time point for each organ were detected from the secondary data matrix. (vi) The genes with relative log ratios commonly greater than 0.75 or uniformly smaller than −0.75 in each organ among at least five individual rats, which had an identical anesthetic period (2 h or 6 h), were selected from the secondary data matrix.

Next, we extracted genes, in which expression patterns were specific to a single organ or common to multiple organs from the secondary data matrix by the following operations. (i) The mean average of log ratios for 2 h or 6 h for each organ (designated 2-h and 6-h averages) was calculated. (ii) The relative ratios of 2-h and 6-h averages against 0-h average for each organ (designated relative 2-h and 6-h averages) were generated. (iii) Genes with relative 2-h average or relative 6-h average greater than 0.75 or lower than −0.75 in a single organ were selected. (iv) Genes with relative 2-h average or relative 6-h average greater than 0.75 or lower than −0.75 in any two organs were selected. (v) Genes with relative 2-h average or relative 6-h average was greater than 0.75 or lower than −0.75 in any three organs were selected. (vi) Genes with relative 2-h average or relative 6-h average greater than 0.75 or lower than −0.75 in any four organs were selected. (vii) Genes with relative 2-h average or relative 6-h average greater than 0.75 or lower than −0.75 in more than four organs were selected.

3. Results

In order to comprehensively evaluate the influences of general anesthesia at the gene expression level, we obtained seven major organs from rats under general anesthesia with sevoflurane, an inhalation anesthetic, at 0 h, 2 h, and 6 h after induction of anesthesia. We performed the animal experiment with sevoflurane twice with an interval of several weeks between the two experiments (designated as Exp. 1 and Exp. 2). In Exp. 1, we used three rats for each time point and obtained for the seven organs but failed to draw peripheral blood from a rat assigned for 2 h. In Exp. 2, we used four rats for 0 h and three rats for 2 h and 6 h, respectively, and failed tissue lysate preparation from the lungs and liver of a rat assigned for 0 h. Eventually, we obtained 130 independent tissue samples for the three time points. We labeled poly(A)+ RNA purified from the samples and a rat common reference RNA with Cyanine-5 and Cyanine-3, respectively, and hybridized to microarrays representing 11,464 transcripts derived from 10,490 individual genes. Hybridization signals were processed into expression ratios as $\log_2$ values (designated log ratios) and compiled into a matrix designated as the primary data matrix (see Materials and methods). Data from all the arrays used in this paper are available at DDBJ via CIBEX (http://www.cibex.nig.ac.jp/cibex/HTML/index.html) under accession numbers CBX4 (for the array design) and CAR4 (for the experiments).

3.1. Overview of gene expression patterns in rat tissues after being subjected to general anesthesia

First, we sought to seize an overview of the experiments conducted in this study by two-dimensional clustering analysis of log ratios calculated from primary expression ratios against the common reference RNA (primary data matrix), prior to extracting genes that were affected by inhalation anesthesia at the expression level. The primary data matrix should enable us to relatively compare all samples one another without conducting direct comparison by hybridization on an identical microarray. We predicted that the most obvious differences obtained from the clustering analysis of the primary data matrix should be those reflecting tissues examined in this study, represented as sample clusters consisting of each organ only (tissue clusters) in a single dendrogram. Furthermore, we presumed that we might be able to compare gene expression levels that were associated with different experimental conditions within each tissue cluster in the dendrogram.

We extracted genes with log ratios over 1 or under −1 in at least one sample from the primary data matrix and subjected them to two-dimensional hierarchical clustering analysis for samples and genes (Fig. 1) (Schena et al., 1996; Lyons et al., 2000). When the clustering analysis for the samples was performed, the greatest seven clusters corresponding to the individual organs were obtained as predicted. The clusters representing the lungs, heart, liver, and blood comprised two smaller clusters completely corresponding to differences between Exp. 1 and Exp. 2, reflecting experimental errors. The clusters representing the kidney and brain consisted of two smaller clusters that incompletely corresponded to the experiment differences with some exceptions. With the exception of the smaller cluster in Exp. 1, representing the liver, in which three

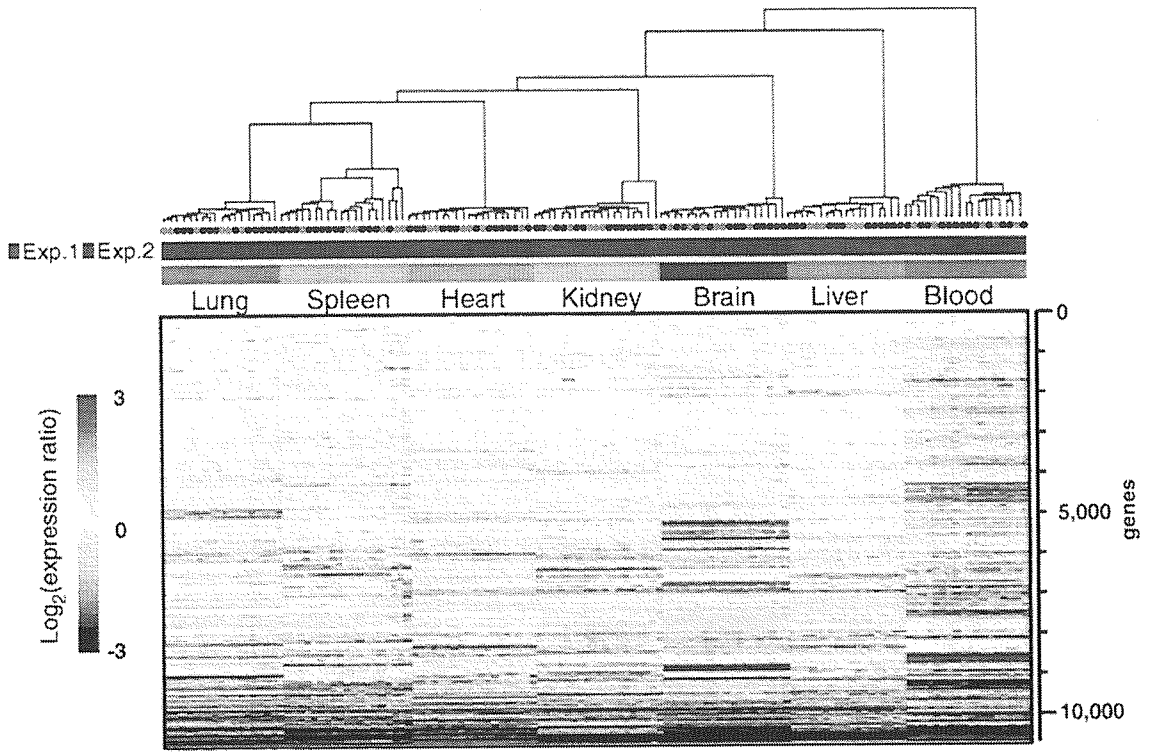

Fig. 1. Gene expression profiles obtained from seven organs of rats under inhalation anesthesia. Rows and columns represent genes (10,796) and samples (130), respectively. The genes and samples are assembled in the order obtained from the results of the two-dimensional hierarchical clustering analysis. Dendrogram at the top of the figure indicates the relationship among the samples after clustering analysis; the y-axis of the dendrogram depicts Euclid square distance as the dissimilarity coefficient. The color bar on the left side of the figure shows expression ratio against the common reference RNA in $\log_2$; red and blue indicate increase and decrease of the expression ratios, respectively. Solid circles indicate individual rats assigned for 0 h, 2 h, and 6 h by black, green, and red, respectively. Red and blue bars show two independent anesthesia experiments, i.e., Exp. 1 and Exp. 2, respectively. Color bars in pink, light blue, orange, violet, dark blue, light green, and gray represent the lungs, spleen, heart, kidney, brain, liver, and blood, respectively.

different time points formed the three smallest clusters, the smaller clusters by the differences in experiment were not divided by differences of anesthetic periods but by the individual differences among rats. These results obtained from the clustering analysis for the 130 samples indicate that differences among anesthesia periods with regard to the expression profiles of over 10,000 genes are much smaller than differences among individual rats, independent experiments, and organs.

3.2. Selection of genes in which expression patterns were affected by inhalation anesthesia

In order to extract genes in which expression levels altered specifically due to inhalation anesthesia, from the primary data matrix, we conducted the operations described in the Materials and methods and generated the secondary data matrix comprising relative log ratios. From the secondary data matrix, we successfully obtained 177 transcripts originating from 167 genes that satisfied the conditions described in the Materials and methods and subsequently subjected the data of the 177 transcripts to clustering analysis for genes (Fig. 2). Clustering analysis demonstrated that the 167 genes comprised those genes specific to a single organ and common in different organs. It also demonstrated that among the organs tested in this study, expression alteration of 114 genes was predominantly detected in the liver and that of 42 genes was predominantly detected in the lungs and the expression alteration of a few genes was predominantly detected in the blood, brain, heart, kidney, and spleen. Moreover, we noticed that the alteration of expression levels was detected mainly in the longer period but rarely in the shorter period. These results confirm that the inhalation anesthesia affected expression of a small number of genes except for the liver. This result was also confirmed by the two-dimensional clustering analysis for the primary data matrix of over 10,000 genes.

3.3. Expression profiles for genes that are immediately affected by anesthesia

Next, we extracted genes whose expression levels were immediately affected by the inhalation anesthesia, particularly in the shorter period by filtering operations similar to those described above. The reason was the following. Although we noticed that the predominant alteration appeared at the time point of 6 h, we expected the possibility that the data obtained at 2 h might provide information on genes that may specifically regulate the expression of the

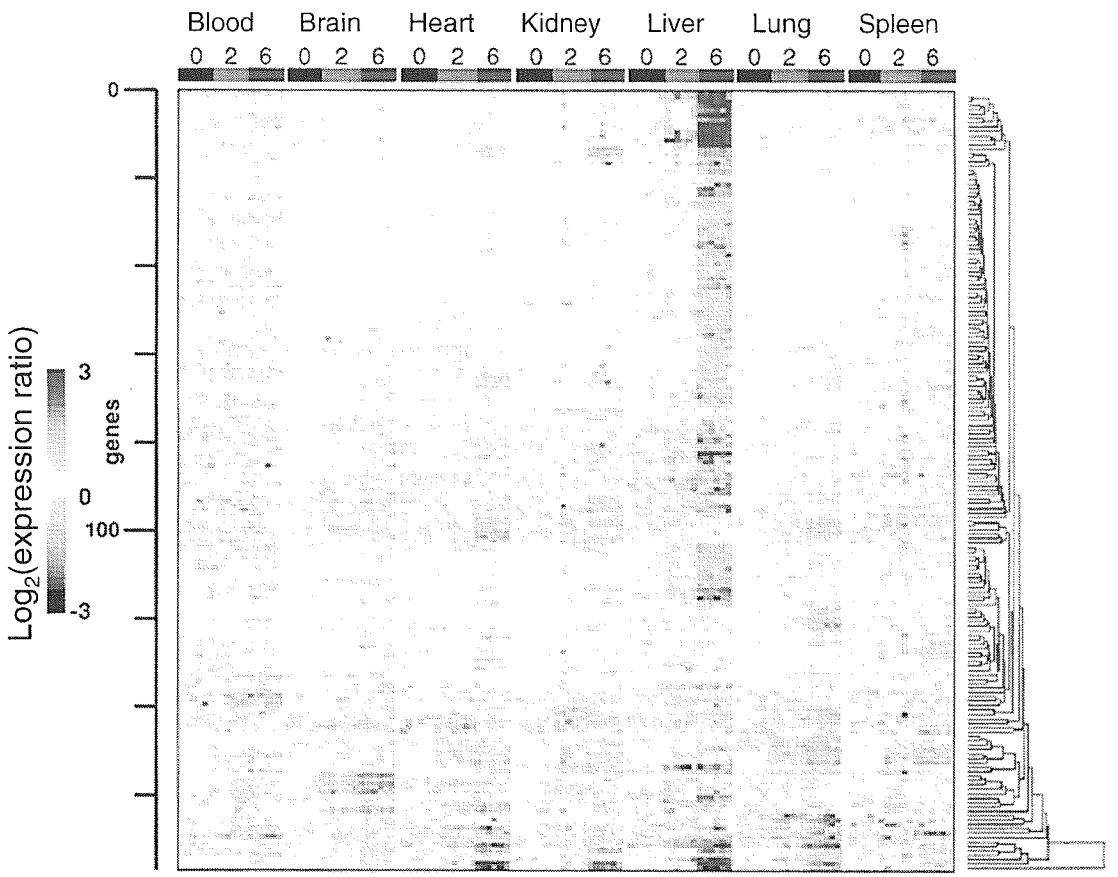

Fig. 2. Clustering analysis of genes in which expression levels were obviously altered in an inhalation anesthesia-specific manner. Rows and columns represent genes and samples, respectively. Rows are assembled in the order derived from clustering analysis. Columns are assembled in the order of organs and time points; black, green, and red bars exhibit 0-h, 2-h, and 6-h samples, respectively. Dendrogram on the right side of the figure indicates the relationship of genes after clustering. The color bar on the left side of the figure shows expression ratio against the common reference RNA in $\log_2$; red and blue indicate increase and decrease of the expression ratios, respectively. Color bars in pink, light blue, orange, violet, dark blue, light green, and gray represent the lungs, spleen, heart, kidney, brain, liver, and blood, respectively.

genes affected in the later phase. We obtained only 20 transcripts derived from 18 genes, as genes affected immediately by the inhalation anesthesia (Fig. 3). These results indicate that in the early phase, an extremely small number of genes are affected by inhalation anesthesia (approximately 0.17% of the total genes tested). Among the 20 transcripts, 18 exhibited single organ-specific expression patterns but only two represented those common in multiple organs. One of the two genes common to the multiple organs was a gene previously known as the circadian gene, *Rev-ErbA-alpha* (Leloup and Goldbeter, 2003). We notice that the gene expressing vasoconstrictor endothelin 1 (Yanagisawa et al., 1988) was upregulated as an early responsive gene in the lungs. This may be because inhalation anesthetics are initially exposed at the highest concentration to the lungs as compared to the otherorgans.

3.4. Extraction of genes in which expression was influenced by inhalation anesthesia in an organ-specific manner

We extracted genes in which expression patterns were specific to a single organ or common in different organs by the operations described in the Materials and methods. Subsequently, we selected genes that satisfied the conditions described in the Materials and methods from the genes shown in Fig. 2. We classified the selected genes in which the expression patterns were influenced by the inhalation anesthesia, as shown in Fig. 4a–e.

In the liver, we detected the maximum number of genes in which the expression was influenced by the inhalation anesthesia (99 transcripts; approximately 56% of the total genes influenced). These liver-specific genes include those characterized as the drug metabolism-associated or the drug response-associated genes such as cytochrome *P*450s (Lu, 1998), epoxide hydrolases (Cannady et al., 2002), UDP-glucuronosyl transferases (Mackenzie et al., 1997), and glutathione sulfotransferases (Snyder and Maddison, 1997). We obtained the second highest number of influenced genes in the lungs (15 transcripts). Since anesthetics act on the brain and induce unconsciousness, we focused on the genes in which the expression specifically influenced the brain. We did not observe an elevation of expression levels of any genes in the brain but detected four genes in which expression levels decreased after the induction of the inhalation

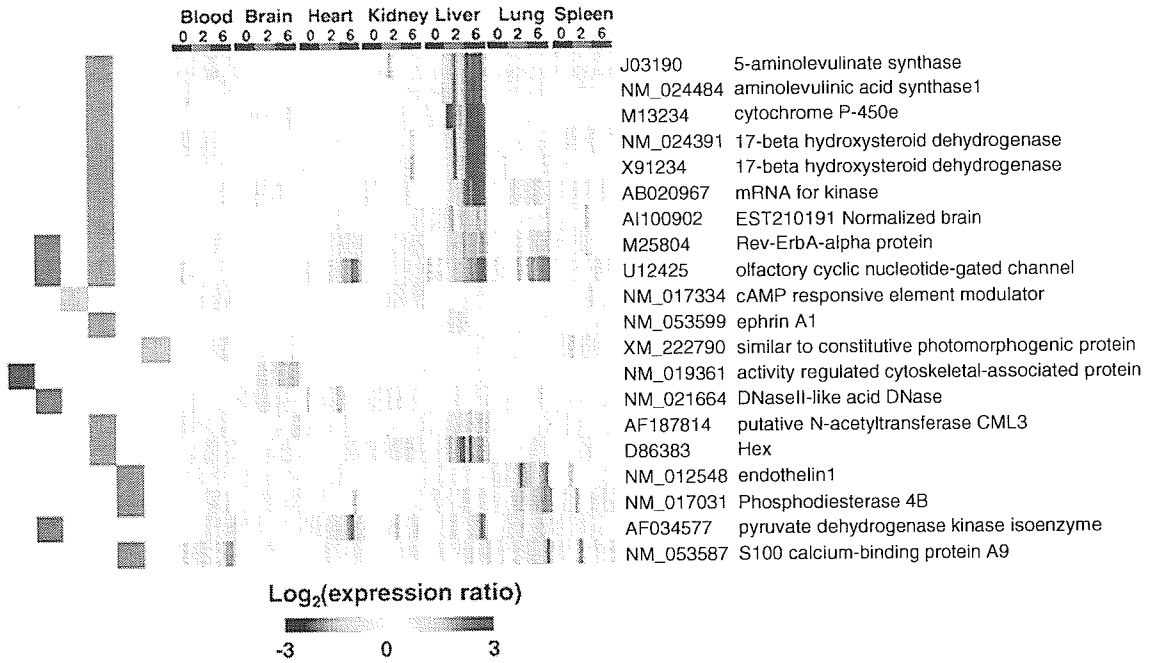

Fig. 3. Genes in which expression levels altered in the early phase (2 h) of inhalation anesthesia. The genes are assembled in the order obtained from the results of hierarchical clustering analysis. The color bar at the bottom of the figure shows expression ratio against the common reference RNA in $\log_2$; red and blue indicate increase and decrease of the expression ratios, respectively. Color bars in pink, light blue, orange, violet, dark blue, light green, and gray represent the lungs, spleen, heart, kidney, brain, liver, and blood, respectively.

anesthesia (*Arc* (Link et al., 1995), *NGFI-B* (Maruyama et al., 1998), *Krox20* (Bhat et al., 1992), and *Egr1* (Liu et al., 1996)). These four genes were previously reported to encode transcription factors and to be those in which the expression levels were differently affected by treatment with the agents acting on the central nervous system (CNS), such as amphetamine (Gonzalez-Nicolini and McGinty, 2002), cocaine (Freeman et al., 2002), pentobarbital (Ryabinin et al., 2000), and antidepressants (Pei et al., 2003).

3.5. Evaluation of genes in which expression was altered during inhalation anesthesia in a multiple organ-common manner

As described above, we notice that several genes were affected during anesthesia in a similar manner among multiple organs. These included the previously reported circadian genes in which the expression level alters with an oscillating rhythm based on whether it is day or night. We selected expression data for the representative circadian genes from the secondary data matrix (Fig. 5). Most temporal expression patterns for known circadian genes obtained in this study were consistent with those reported previously with the exception of the genes from the brain (Ueda et al., 2002; Storch et al., 2002; Panda et al., 2002). In the brain, we observed no alteration of the expression of the known circadian genes during anesthesia with the exception of *Per2*. The *Per2* gene provided an expression pattern contradictory to those reported previously, representing decreased expression levels during the day. Furthermore, we compared expression patterns obtained in this study with those recently reported for the mouse circadian genes using the microarray technology (Ueda et al., 2002). The rat orthologues of the mouse circadian genes in the brain exhibited no alteration of expression during the inhalation anesthesia. The genes compared will be listed in Supplementary Information Table 6 (http://www.cibex.nig.ac.jp/cibex/HTML/index.html; under accession no. CAR4). These findings indicate that under inhalation anesthesia, the circadian rhythm may differ from normal circadian rhythms.

4. Discussion

By analyzing expression profiles obtained from rats under general anesthesia,we have shown that inhalation anesthesia affected expression of a small number of genes.

Fig. 4. Classification of genes that showed alteration in expression levels during anesthesia by the number of the organs in which the alteration was detected. a, genes in which expression levels altered in a single organ-specific manner. The genes of each gene set for a specific organ are assembled in the order derived from clustering. b, c, d, e, and f, genes in which expression levels altered commonly in two, three, four, and more than four organs, respectively. The color bar at the bottom of the figure shows expression ratio against the common reference RNA in $\log_2$; red and blue indicate increase and decrease of the expression ratios, respectively. Color bars in pink, light blue, orange, violet, dark blue, light green, and gray represent the lungs, spleen, heart, kidney, brain, liver, and blood, respectively.

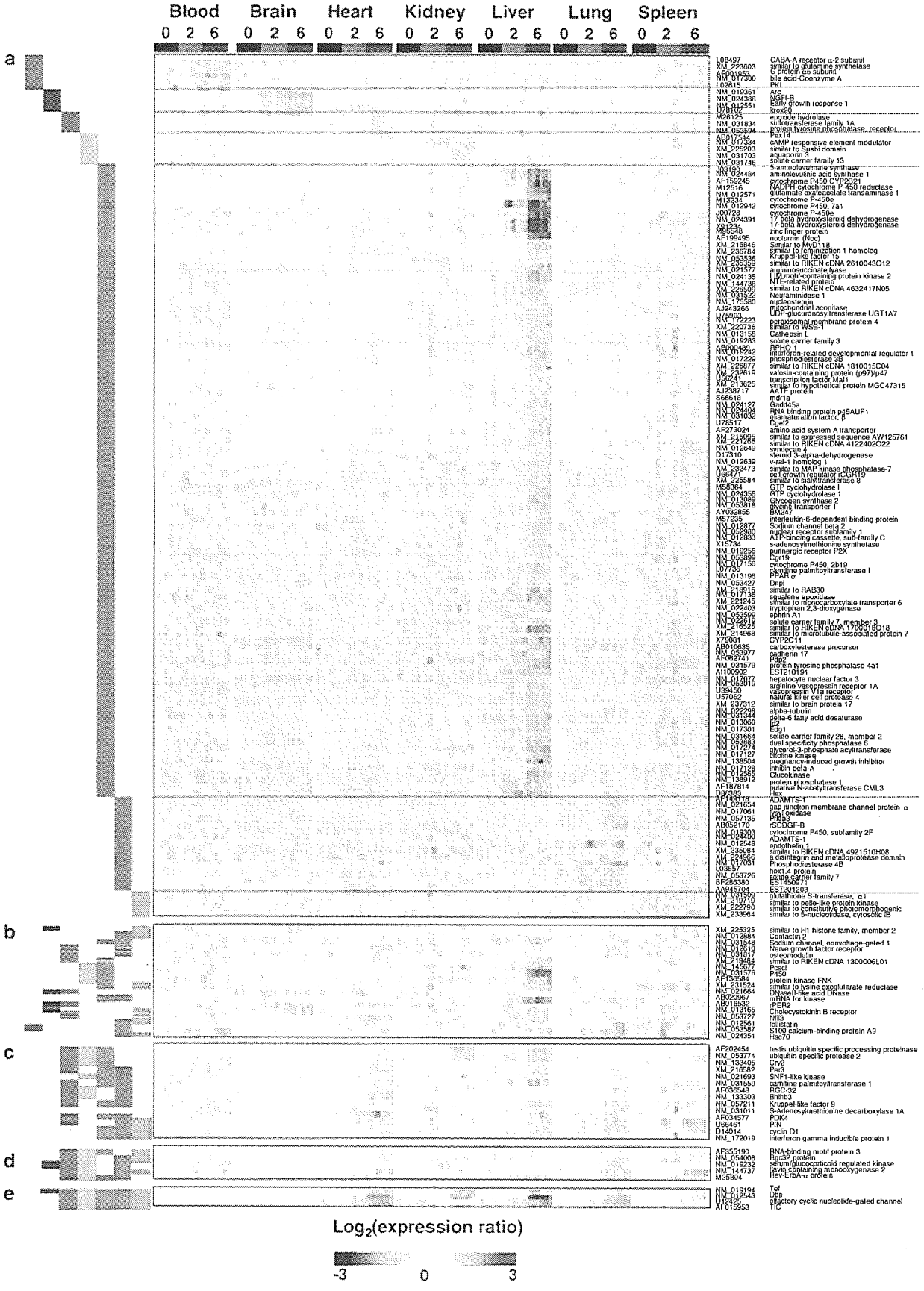
Blood
Brain
Heart
Kidney
Liver
Lung
Spleen
0 2 6
a
b
c
d
e
Log2(expression ratio)
-3
0
3

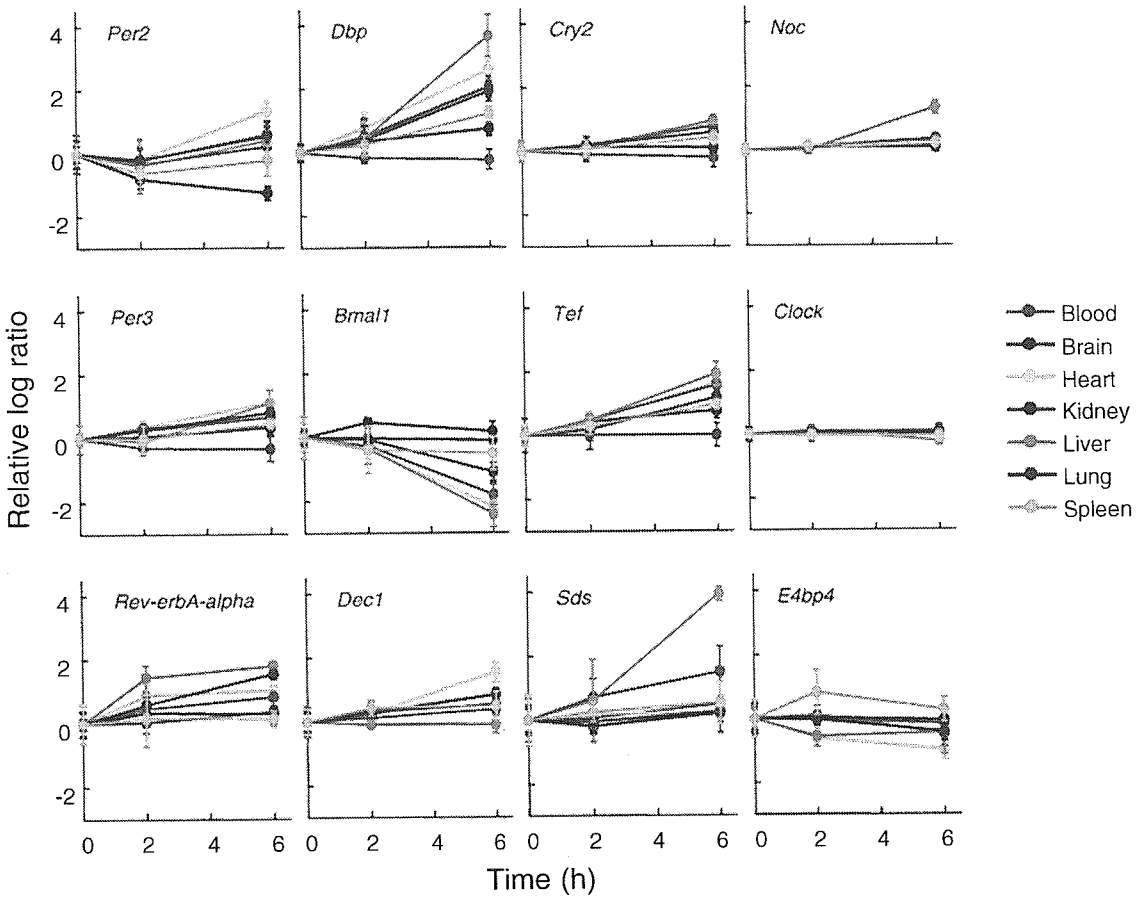

Fig. 5. Expression kinetics of the rat orthologues for the previously identified mouse circadian genes in rats under inhalation anesthesia. Relative log ratios were extracted from the secondary data matrix for the following genes: *Clock*, *Per2*, *Cry2*, *Per3*, *Noc*, *Tef*, *Rev-erbA-alpha*, *Dbp*, and *Bmal1*. The extracted relative log ratios were subjected to calculation of mean average (solid circle) and standard deviation (error bar) for each time point of individual organs. The x and y axes show time (h) and relative log ratio against the 0-h control, respectively. Graphs in pink, light blue, orange, violet, dark blue, light green, and gray represent the lungs, spleen, heart, kidney, brain, liver, and blood, respectively.

Our study should provide the first comprehensive assessment for the influence of inhalation anesthesia with regard to experimental biology and genome science. Although we did not observe obvious alterations for the majority of genes tested, we successfully detected genes in which expression levels were influenced in an inhalation anesthesia-dependent manner.

Among the genes in which expression levels altered in an anesthesia-dependent manner, the most predominant gene cluster was found in the samples obtained from the liver. The genes will be listed in Supplementary Information Table 4 (http://www.cibex.nig.ac.jp/cibex/HTML/index.html; under accession no. CAR4). These liver-specific genes include many cytochrome *P*450s, UDP-glucuronosyl transferases, and glutathione sulfotransferases, representing involvement and activation of drug-metabolizing enzyme systems by hydroxylation, glucuronide conjugation, and glutathione conjugation, respectively (Lu, 1998; Cannady et al., 2002; Mackenzie et al., 1997; Clarke et al., 1997). This indicates that almost all the genes in the enzyme systems previously identified to be involved in drug metabolism in the liver are engaged (Gerhold et al., 2001). However, it is rather predictable that an inhalation anesthetic induces the expression of the drug metabolism-related genes as a toxicological response. On the other hand, as novel findings, our data propose that many transcripts (thus far uncharacterized) may be regulated by a common set of trasncription factors, in addition to being involved in the metabolism of the anesthetic in a similar manner to the genes for drug-metabolizing enzymes that were previously identified. Moreover, we presume that the induction of endothelin at the early phase of anesthesia in the lungs represents one of the toxicological responses and that endothelin possibly induces some effects in the vascular system, particularly in the early phase of the anesthetic period. This is presumed because the induction of the endothelin gene expression has been previously reported as responses to toxins (Sonin et al., 1999; Baveja et al., 2002). It needs to be investigated whether other anesthetics affect the expression of the genes in a manner similar to sevoflurane, as demonstrated in this study. Such a comparative study would provide information that is necessary to assess the side effects of the currently available anesthetics and to develop safe tools in anesthesiology.

We should mention that the findings presented here may not provide direct evidence to suggest that the anesthetic causes the anesthetic status by inducing alteration in the expression of certain genes since we did not detect many regulated genes in the brain, which should comprise the main target of the anesthetic. Despite the low number of regulated genes (3 up, 6 down), these genes encode transcription factors and circadian rhythm genes that were previously reported to be increased by amphetamine (Gonzalez-Nicolini and McGinty, 2002), cocaine (Freeman et al., 2002), and morphine withdrawal (Ammon et al., 2003), whereas their expression decreases by anesthesia with an intravenous anesthetic (Ryabinin et al., 2000).

One of the interesting findings of this study is that several circadian genes exhibited alteration of expression during an anesthetic period in a multiple organ-common manner. However, in the brain, we obtained several findings that were inconsistent with those reported previously (Ueda et al., 2002). We did not detect an alteration in several genes in which expression exhibited the circadian rhythm and we observed contradictory kinetics in the expression of *Per2*. The hypothesis that inhalation anesthesia perturbs the circadian rhythms requires further investigations. We assume that one of the reasons for these differences may be due to the tissue used for analysis. Most previous studies focused on the center of the circadian rhythm, the suprachiasmatic nucleus (Ueda et al., 2002; Panda et al., 2002). On the other hand, we used the whole brain as a target. The suprachiasmatic nucleus occupies an extremely small region of the whole brain. Therefore, the dilution of mRNA of the suprachiasmatic nucleus with mRNA of the whole brain might have affected the detection of the expression of the circadian genes mainly regulated in the suprachiasmatic nucleus. Furthermore, to obtain conclusive evidence for the association of anesthetic periods and the expression of circadian genes, future studies should scrutinize expression profiles for circadian genes at more multiple time points with a shorter interval than those used in this study. In order to further analyze the circadian gene expression, it would be useful to perform a non-microarray approach such as real-time PCR for the limited number of target genes as shown in this study.

In this study, we independently repeated the identical anesthetic experiment twice with rats. Clustering analysis shown in Fig. 1 exhibits that with the exception of the brain and kidney, in the other five organs smaller clusters are generated for each, which correspond to the two independent anesthetic experiments, reflecting experimental errors. Only the brain and kidney do not exhibit such smaller clusters that completely corresponded to the two independent experiments, indicating that in these two organs, experimental errors between the two experiments were smaller than the differences among individual rats and/or experimental conditions for anesthesia. These results clearly indicate that experimental errors among independent anesthetic experiments are not negligible and that one should be careful while drawing conclusions from a single experiment with animals under mildly different experimental conditions such as inhalation anesthesia. We successfully avoided highlighting genes that reflected the experimental errors by repeating the identical anesthetic experiments and conducting filtering operations for a combined gene expression data set. These findings provide experimental evidence that endorses the significance of repeating an independent experiment with animals under experimental conditions with mild differences and of data processing to reduce noises that reflect the differences among the repeated experiments.

As described above, our study demonstrates that the experimental errors observed between the independently repeated anesthetic experiments provided the second highest difference that follows the differences among the individual organs tested, which generated the most distinguishable clusters. This finding led us to use threshold-based approaches with strict cutoff values to extract genes in which expression was specifically affected by inhalation anesthesia and to avoid influence of the experimental errors and the differences among individual rats assigned for the identical conditions. These relatively strict analytical approaches may result in insufficient extraction of specifically affected genes, particularly for those in which expression was altered in a subtle manner. One of the analytical approaches that may enable us to obtain a greater number of genes specifically affected by inhalation anesthesia should be to apply lower thresholds in the filtering operation described in the Materials and methods for the data set compiled in this study. The approach may be effective to obtain as much information as possible from our primary data set. However, this would require additional confirmation for the individual values through non-microarray approaches.

We have provided a large and powerful data set for exploring the influence of inhalation anesthesia in rats. The entire data set will be available in a public database. The results presented here were derived from the data set by relatively conservative approaches due to the experimental differences greater than those expected prior to data analysis. Therefore, apart from conducting additional more fine-tuned experiments, another approach may be helpful for the further understanding of comprehensive influence of anesthesia by means of utilizing advanced statistical methods such as analysis of variance (ANOVA). Application of the more sophisticated approaches would enable those who use the data set to explore additional categories of genes that are modulated under anesthesia.

Acknowledgments

We thank K. Kon, S. Nakajima, and S. Nakamura for technical assistance.

Appendix A. Supplementary data

Supplementary data associated with this article can be found, in the online version, at doi:10.1016/j.gene.2005.03.022.

References

Ammon, S., Mayer, P., Riechert, U., Tischmeyer, H., Hollt, V., 2003. Microarray analysis of genes expressed in the frontal cortex of rats chronically treated with morphine and after naloxone precipitated withdrawal. Brain Res. Mol. Brain Res. 112, 113–125.

Baveja, R., Keller, S., Yokoyama, Y., Sonin, N., Clemens, M.G., Zhang, J.X., 2002. LPS-induced imbalanced expression of hepatic vascular stress genes in cirrhosis: possible mechanism of increased susceptibility to endotoxemia. Shock 17, 316–321.

Bhat, R.V., Worley, P.F., Cole, A.J., Baraban, J.M., 1992. Activation of the zinc finger encoding gene krox-20 in adult rat brain: comparison with zif268. Brain Res. Mol. Brain Res. 13, 263–266.

Brown Jr., B.R., Frink, E.J., 1993. The safety of sevoflurane in humans. Anesthesiology 79, 201–202.

Cannady, E.A., Dyer, C.A., Christian, P.J., Sipes, I.G., Hoyer, P.B., 2002. Expression and activity of microsomal epoxide hydrolase in follicles isolated from mouse ovaries. Toxicol. Sci. 68, 24–31.

Clarke, H., et al., 1997. Alpha-gluthathione *S*-transferase (alpha-GST) release, an early indicator of carbon tetrachloride hepatotoxicity in the rat. Hum. Exp. Toxicol. 16, 154–157.

Forrest, J.B., et al., 1990. Multicenter study of general anesthesia: I. Design and patient demography. Anesthesiology 72, 252–261.

Franks, N.P., Lieb, W.R., 1994. Molecular and cellular mechanisms of general anaesthesia. Nature 17, 607–614.

Freeman, W.M., et al., 2002. Changes in rat frontal cortex gene expression following chronic cocaine. Brain Res. Mol. Brain Res. 104, 11–20.

Gerhold, D., Lu, M., Xu, J., Austin, C., Caskey, C.T., Rushmore, T., 2001. Monitoring expression of genes involved in drug metabolism and toxicology using DNA microarrays. Physiol. Genomics 5, 161–170.

Gonzalez-Nicolini, V., McGinty, J.F., 2002. Gene expression profile from the striatum of amphetamine-treated rats: a cDNA array and in situ hybridization histochemical study. Gene Expr. Patterns 1, 193–198.

Harris, R.A., Mihic, S.J., Dildy-Mayfield, J.E., Machu, T.K., 1995. Actions of anesthetics on ligand-gated ion channels: role of receptor subunit composition. FASEB J. 9, 1454–1462.

Ito, E., et al., 2003. A tetraspanin-family protein, T-cell acute lymphoblastic leukemia-associated antigen 1, is induced by the Ewing's sarcoma–Wilms' tumor 1 fusion protein of desmoplastic small round-cell tumor. Am. J. Pathol. 163, 2165–2172.

Kobayashi, S., et al., 2004. Dynamic regulation of gene expression by the Flt-1 kinase and Matrigel in endothelial tubulogenesis. Genomics 84, 185–192.

Leloup, J.C., Goldbeter, A., 2003. Toward a detailed computational model for the mammalian circadian clock. Proc. Natl. Acad. Sci. U. S. A. 100, 7051–7056.

Levy, W.J., 1984. Clinical anaesthesia with isoflurane. A review of the multicentre study. Br. J. Anaesth. 56, 101S–112S.

Link, W., et al., 1995. Somatodendritic expression of an immediate early gene is regulated by synaptic activity. Proc. Natl. Acad. Sci. U. S. A. 92, 5734–5738.

Liu, C., Calogero, A., Ragona, G., Adamson, E., Mercola, D., 1996. EGR-1, the reluctant suppression factor: EGR-1 is known to function in the regulation of growth, differentiation, and also has significant tumor suppressor activity and a mechanism involving the induction of TGF-beta1 is postulated to account for this suppressor activity. Crit. Rev. Oncog. 7, 101–125.

Lu, A.Y., 1998. Drug-metabolism research challenges in the new millennium: individual variability in drug therapy and drug safety. Drug Metab. Dispos. 26, 1217–1222.

Lyons, T.J., Gasch, A.P., Gaither, L.A., Botstein, D., Brown, P.O., Eide, D.J., 2000. Genome-wide characterization of the Zap1p zinc-responsive regulon in yeast. Proc. Natl. Acad. Sci. U. S. A. 97, 7957–7962.

Mackenzie, P.I., et al., 1997. The UDP glycosyltransferase gene superfamily: recommended nomenclature update based on evolutionary divergence. Pharmacogenetics 7, 255–269.

Maruyama, K., Tsukada, T., Ohkura, N., Bandoh, S., Hosono, T., Yamaguchi, K., 1998. The NGFI-B subfamily of the nuclear receptor superfamily (review). Int. J. Oncol. 12, 1237–1243.

Panda, S., et al., 2002. Coordinated transcription of key pathways in the mouse by the circadian clock. Cell 109, 307–320.

Pei, Q., Zetterstrom, T.S., Sprakes, M., Tordera, R., Sharp, T., 2003. Antidepressant drug treatment induces Arc gene expression in the rat brain. Neuroscience 121, 975–982.

Ryabinin, A.E., Wang, Y.M., Bachtell, R.K., Kinney, A.E., Grubb, M.C., Mark, G.P., 2000. Cocaine- and alcohol-mediated expression of inducible transcription factors is blocked by pentobarbital anesthesia. Brain Res. 877, 251–261.

Schena, M., Shalon, D., Heller, R., Chai, A., Brown, P.O., Davis, R.W., 1996. Parallel human genome analysis: microarray-based expression monitoring of 1000 genes. Proc. Natl. Acad. Sci. U. S. A. 93, 10614–10619.

Snyder, M.J., Maddison, D.R., 1997. Molecular phylogeny of glutathione-*S*-transferases. DNA Cell Biol. 16, 1373–1384.

Sonin, N.V., Garcia-Pagan, J.C., Nakanishi, K., Zhang, J.X., Clemens, M.G., 1999. Patterns of vasoregulatory gene expression in the liver response to ischemia/reperfusion and endotoxemia. Shock 11, 175–179.

Storch, K.F., et al., 2002. Extensive and divergent circadian gene expression in liver and heart. Nature 417, 78–83.

Ueda, H.R., et al., 2002. Transcription factor response element for gene expression during circadian night. Nature 418, 534–539.

Yanagisawa, M., et al., 1988. A novel potent vasoconstrictor peptide produced by vascular endothelial cells. Nature 332, 411–415.

International Immunology, Vol. 18, No. 1, pp. 183–198
doi:10.1093/intimm/dxh361

Peptide-induced immune protection of CD8$^+$ T cell-deficient mice against Friend retrovirus-induced disease

Hiroyuki Kawabata[1], Atsuko Niwa[1,3], Sachiyo Tsuji-Kawahara[1], Hirohide Uenishi[2], Norimasa Iwanami[1,4], Hideaki Matsukuma[1], Hiroyuki Abe[1], Nobutada Tabata[1,5], Haruo Matsumura[1] and **Masaaki Miyazawa[1]**

[1]Department of Immunology, Kinki University School of Medicine, 377-2 Ohno-Higashi, Osaka-Sayama, Osaka 589-8511, Japan
[2]Genome Research Department, National Institute of Agrobiological Science, Tsukuba, Ibaraki 305-8602, Japan

[3]Present address: Department of Pharmacology, Kinki University School of Medicine, Osaka-Sayama, Osaka 589-8511, Japan
[4]Present address: Division of Experimental Immunology, Institute for Genome Research, University of Tokushima, Tokushima 770-8503, Japan
[5]Present address: Department of Pediatrics, Kinki University School of Medicine, Osaka-Sayama, Osaka 589-8511, Japan

Keywords: B cell-deficient, β_2-microglobulin-deficient, CD4$^+$ T, epitope, vaccine

Abstract

CD8$^+$ CTLs and virus-neutralizing antibodies have been associated with spontaneous and vaccine-induced immune control of retroviral infections. We previously showed that a single immunization with an *env* gene-encoded CD4$^+$ T cell epitope protected mice against fatal Friend retrovirus infection. Here, we analyzed immune cell components required for the peptide-induced anti-retroviral protection. Mice lacking CD8$^+$ T cells were nevertheless protected against Friend virus infection, while mice lacking B cells were not. Virus-producing cells both in the spleen and bone marrow decreased rapidly in their number and became undetectable by 4 weeks after infection in the majority of the peptide-immunized animals even in the absence of CD8$^+$ T cells. In the vaccinated animals the production and class switching of virus-neutralizing and anti-leukemia cell antibodies were facilitated; however, virus-induced erythroid cell expansion was suppressed before neutralizing antibodies became detectable in the serum. Further, the numbers of virus-producing cells in the spleen and bone marrow in the early stage of the infection were smaller in the peptide-immunized than in unimmunized control mice in the absence of B cells. Thus, peptide immunization facilitates both early cellular and late humoral immune responses that lead to the effective control of the retrovirus-induced disease, but CD8$^+$ T cells are not crucial for the elimination of virus-infected cells in the peptide-primed animals.

Introduction

Understanding the types of immune responses associated with and responsible for effective control of viral infection is pivotal for the development of antiviral vaccines. We, along with other researchers, have been studying the requirements of different immune cell components and their regulation by host genetic factors utilizing the mouse model of Friend retrovirus infection. Friend retrovirus complex (FV) is composed of replication-competent Friend murine leukemia virus (F-MuLV) and defective spleen focus-forming virus (SFFV), the latter of which induces rapid growth and terminal differentiation of infected erythroid progenitor cells (1, 2). FV is known to induce fatal erythroleukemia associated with severe immunosuppression when inoculated into immunocompetent adult mice of susceptible strains (1, 3). Genotypes at both MHC class I and class II loci, along with those at a non-MHC locus located on chromosome 15, affect spontaneous immune resistance against FV-induced disease development which is phenotypically manifested by the regression of early splenomegaly and clearance of viremia (1, 4–8). As predicted, requirements of both CD4$^+$ and CD8$^+$ T cells for the above

Correspondence to: M. Miyazawa; E-mail: masaaki@med.kindai.ac.jp

Transmitting editor: K. Sugamura

Received 4 June 2005, *accepted* 28 October 2005

Advance Access publication 13 December 2005

spontaneous resistance have been demonstrated through antibody-mediated depletion of T cell subsets and through the blocking of T cell responses by administration of anti-MHC class II antibodies (9, 10). Further, different roles of $CD4^+$ and $CD8^+$ T cells and of virus-neutralizing antibodies have been demonstrated for immune protection against FV infection induced with a live attenuated vaccine (11, 12).

We previously showed that a single immunization with an 18-mer peptide that contains a single $CD4^+$ T cell epitope identified within the *env* gene product SU of F-MuLV induces strong protective immunity against fatal FV infection in susceptible strains of mice (13, 14). In peptide-immunized (B10.A × A.BY)F_1 mice, the vast majority of virus-producing cells were eliminated from the spleen between 8 and 12 days after FV challenge, and the SFFV-induced early splenomegaly regressed rapidly. Production and class switching of virus-neutralizing antibodies roughly coincided with the above reduction in the number of virus-producing cells in the spleen (13), suggesting the possible importance of virus-neutralizing antibodies in the vaccine-induced confinement of FV infection. However, since the activation of both $CD4^+$ and $CD8^+$ cytotoxic effector cells and of NK cells was detectable prior to the decrease of virus-producing cells in peptide-immunized (BALB/c × C57BL/6)F_1 ($CB6F_1$) mice (14), it was also possible that the cellular responses, rather than the antibodies, were mainly responsible for the control of FV-induced disease development conceivably through the destruction of virus-producing cells. Moreover, since $CD8^+$ CTLs and NK cells were activated in comparable degrees both in peptide-immunized and unimmunized animals after FV infection (14), their actual extents of contribution to the peptide-induced immune protection remained unclear.

To directly evaluate the role of each separate immune cell component in peptide-induced protection against FV infection and to compare the effector mechanisms induced by the peptide immunization with those induced by previously described live attenuated vaccines (11, 15), we performed the protection experiments on the highly susceptible strain of mice that lacked either $CD8^+$ T or B lymphocytes.

Methods

Mice

BALB/c-AJcl and $CB6F_1$ mice were purchased from Japan SLC, Inc., Hamamatsu, Japan. (B10.A × A.BY)F_1 mice were those described previously (13). Breeding pairs of BALB/c-J-*B2m*^{tm1Unc} and C57BL/6J (B6)-*B2m*^{tm1Unc} mice carrying homozygous disruption of the β_2-microglobulin gene ($\beta_2m^{-/-}$) were purchased from the Jackson Laboratory, Bar Harbor, ME, USA, and F_1 crosses were produced at the Animal Facilities, Kinki University School of Medicine. Phenotypic lack of $CD8^+$ T cells in the produced F_1 crosses was confirmed by bleeding each mouse from the tail vein and staining peripheral blood with a mixture of fluorescence-labeled anti-CD4 and anti-CD8 mAbs as described in the following section.

B6-*Igh-6*^{tm1Cgm} mice carrying homozygous disruption of the membrane exon of the Ig μ-chain gene (μ-chain membrane exon-targeted: *μMT/μMT*) and thus lacking B cells (16) were also purchased from the Jackson Laboratory. To introduce the μ-chain disruption into BALB/c background, a cross-intercross production of a congenic strain was performed as follows: the B cell-deficient B6 male mice were mated with BALB/c female mice and F_1 crosses carrying heterozygous disruption of the μ-chain membrane exon were obtained. These heterozygous F_1 crosses were cross-mated, and F_2 mice carrying the homozygous μ gene disruption were selected by performing both genetic and phenotypic analyses as described below. The homozygous disruption of the μ-chain membrane exon in the resulting F_2 crosses was confirmed by PCR analyses as follows: genomic DNA was prepared from the tail tip of each mouse using DNeasy Tissue Kit (Qiagen GmbH, Hilden, Germany) according to the manufacturer's instructions. Oligo-DNA primers (5′ primer: 5′-TCTATCGCCTTCTTGACGAG-3′, 3′ primer: 5′-TACAGCTCAGCTGTCTGTGG-3′) were prepared based on the sequence information on the knockout cassette (16) and were used for PCR amplification of genomic DNA fragments. PCR products were separated by electrophoresis in a 4% agarose gel and were visualized under a UV light after ethidium bromide staining. In addition to the above genetic analyses, peripheral blood was stained with a mixture of fluorescence-labeled anti-CD3 and anti-CD19 mAb, and multicolor flow cytometric analyses were performed as described in the following section. Male F_2 mice carrying homozygous disruption of the μ-chain membrane exon and thus lacking B cells were mated with BALB/c female mice again, and this cross-intercross mating procedure was repeated seven times. After the seventh cycle of crossing and intercrossing, the resultant BALB/c-background mice possessing homozygous disruption of the μ-chain gene were maintained by sister–bother mating, and $CB6F_1$ mice lacking B cells were produced by crossing the B6-*Igh-6*^{tm1Cgm} and the above-established BALB/c-*μMT/μMT* mice.

For immune protection experiments, both male and female mice aged 8–11 weeks at the time of immunization were used throughout the present study. All the animal experiments were approved by the Animal Experiment Committee and performed under the guidelines of Kinki University.

Viruses and their inoculation

A stock of B-tropic FV complex was originally given by Bruce Chesebro, Laboratory of Persistent Viral Diseases, National Institute of Allergy and Infectious Diseases, Hamilton, MT, USA. The stock used in the present study has been described (14, 17). SFFV and F-MuLV titers of the FV stock were determined as described previously (13, 18). For inoculation into $CB6F_1$ mice, a dilution of the virus stock prepared with phosphate-buffered balanced salt solution (PBBS) containing 2% fetal bovine serum (FBS) was injected intravenously into the tail vein. Infected mice were observed at least twice a day and the number of surviving mice was determined. The development of splenomegaly was monitored by palpation as described (5, 17, 19). In some experiments, moribund mice were killed by cervical dislocation and spleen weights were measured to compare the results of palpation with actual spleen weights. Spleens weighing >0.5 g were consistently marked as palpable splenomegaly. Mice found dead were

dissected, and their spleen weight was measured to confirm leukemic death.

Peptide synthesis and immunization

The peptides used for detailed mapping of the $CD4^+$ T cell epitope were synthesized by Fmoc chemistry and purified, and their molecular weight confirmed by quad-polar mass spectrometry as described previously (20–22). Peptides used for immune protection experiments were ordered from Qiagen K. K. (Tokyo, Japan). For immunization each peptide was dissolved in PBBS and emulsified with an equal volume of CFA (Difco Laboratories, Detroit, MI, USA). Mice were injected intradermally with 100 µl of the emulsion given as multiple split doses into the abdominal wall. Control mice were given an emulsion of PBBS and CFA that did not contain any peptide.

T cell proliferation assays

Two T cell clones, F5-5 and FP7-11 (20, 23), specific for the $E^{b/d}$-restricted C-terminal epitope of F-MuLV *env* gene product were maintained as described previously (20). For examination of proliferative responses, 2×10^5 spleen cells irradiated with 40 Gy γ-ray were mixed with 2×10^5 T cells and various concentrations of a peptide in a well of 96-well microculture plates. After 48 h of incubation at 37°C, each culture was pulsed with 18.5 kBq [^{3}H]thymidine (Du Pont NEN, Boston, MA, USA) for the final 18 h. Cells were harvested onto a glass fiber filter, and incorporated radioactivity was measured with a microplate scintillation counter (TopCount, Packard Instrument Co., Meriden, CT, USA). For the calculation of relative stimulatory effect of each peptide, the concentration of peptide i (µM) required to induce 50% of the maximum proliferative response (ED_{50}) was divided with ED_{50} (µM) of the peptide in question (22, 23). In the present study proliferative responses were measured for a range of peptide concentrations between 0.01 and 20 µM in 2-fold dilutions, and peak responses (>30 000 counts per minute) were observed by stimulation with 1 µM of peptide i. ED_{50} of peptide i was 0.2 µM.

Assays for virus-neutralizing antibodies

The *in vitro* assays for quantitative measurement of F-MuLV-neutralizing antibodies have been described elsewhere in detail (5, 13, 17, 19). Mice were bled from the tail vein under ether anesthesia and sera separated were stored at −30°C until use. Stock of an infectious molecular clone of F-MuLV, FB29 (24), was prepared from a high-producer clone of chronically infected *Mus dunni* cells. Serial 2-fold dilutions of sera were made with PBBS containing 1% FBS and mixed with an appropriate dilution of the F-MuLV stock and inoculated to *Mus dunni* cells in 24-well plates. Control wells were inoculated with the virus dilution admixed with the diluent alone. Two days later, foci of F-MuLV-infected cells were visualized with mAb 720 (18) and counted under a dissecting microscope. Neutralizing titers were determined by the reciprocals of maximum dilutions that gave a reduction in the number of F-MuLV-infected cell foci to <25% of those in the control wells. IgG titers were determined by treating each serum sample with 0.05 M 2-mercaptoethanol whereas IgM titers were calculated by dividing the neutralizing titers of the untreated sera by the corresponding IgG titers (6).

Infectious center assays

These assays were performed as described previously (13, 17). Briefly, spleen and bone marrow cell suspensions prepared from mice challenged with FV were serially diluted with PBBS containing 2% FBS, plated in triplicate at concentrations between 30 and 3×10^6 cells per well onto monolayers of *Mus dunni* cells that had been seeded at 1.0×10^4 cells ml^{-1} per well on the previous day and then co-cultured for 2 days. After washing with PBBS and fixation with methanol, F-MuLV-infected cell foci were stained with mAb 720 (18), visualized by using the avidin-biotinylated peroxidase complex (Vector Laboratories, Burlingame, CA, USA) and counted under a magnifier. The numbers of detected foci are in linear correlation with the numbers of spleen cells inoculated in the range between 30 and 3×10^6 cells per well. For the plating of the whole spleen cells from each mouse, 5×10^6 spleen cells per well were added similarly to the previously started culture of *Mus dunni* cells in 20 wells of a 24-well plate, and the remaining spleen cells were diluted and plated at 5×10^5 and 5×10^4 cells per well into separate wells.

Flow cytometry

Flow cytometric analyses of cell-surface markers were performed as described elsewhere (14, 17, 25). Spleen and bone marrow tissues were dissociated in PBBS containing 2% FBS, and a single-cell suspension was prepared by passing each dissociated tissue through a nylon mesh. Cells were stained with a combination of the following mAbs, washed three times with PBBS containing 2% FBS and 0.05% NaN_3 and stained with 20 µg ml^{-1} 7-aminoactinomycin D (7-AAD). 7-AAD was used to exclude dead cells (26). The mAbs and their final concentrations used in the present study were: cychrome-conjugated anti-mouse CD3 (hamster IgG, PharMingen, San Diego, CA, USA) at 0.5 µg per 10^6 cells, FITC-conjugated anti-mouse CD4 (rat IgG2b, Seikagaku Corporation, Tokyo, Japan) at 0.5 µg per 10^6 cells, R-PE-conjugated anti-mouse CD8 (rat IgG2a, Caltag Laboratories, Burlingame, CA, USA) at 1 µg per 10^6 cells, PE-conjugated anti-mouse CD19 (rat IgG2a, PharMingen) at 1 µg per 10^6 cells, FITC-conjugated anti-mouse CD69 (hamster IgG, PharMingen) at 1 µg per 10^6 cells and allophycocyanin-conjugated anti-mouse TER-119 (PharMingen) at 0.2 µg per 10^6 cells. TER-119 reacts with a molecule associated with glycophorin A, and marks the late erythroblasts and mature erythrocytes, but not burst-forming and colony-forming units of erythroid cells (27). Biotinylated mAb 720 (IgG1) and 514 (IgM) used for the detection of F-MuLV gp70 and SFFV gp55, respectively, on infected cell surfaces has been described (13, 17). mAb 34 (IgG2b) reactive with the p15 (MA) protein (28) was similarly purified and biotinylated to detect cell-surface expression of the *gag* gene products (19). All staining reactions were performed in the presence of 0.25 µg per 10^6 cells anti-mouse CD16/CD32 (PharMingen) as described previously (25) to prevent the binding of mAb to FcR-expressing cells. Isotype-matched control antibodies were either purchased from the same suppliers or prepared as purified and biotinylated Ig of an irrelevant specificity as described (25), and staining patterns obtained with the negative-control antibodies were used to draw demarcation lines between cells positively stained and

those not stained. Multicolor flow cytometric analyses were performed with a Becton Dickinson FACSCalibur and CellQuest software (Becton Dickinson Immunocytometry Systems, San Jose, CA, USA). Mature erythrocytes and dead cells were excluded from the analyses by setting a polygonal gate in the dot plots showing intensities of forward scatter and fluorescence for 7-AAD.

Titration of serum antibody reactive to the surface of FV-induced leukemia cells

Sera were serially diluted between 1/4 and 1/256 with PBBS and 100 µl of each dilution was incubated with 10^6 FV-induced leukemia cells Y57-2C ($H2^{b/b}$). Characteristics of the leukemia cell line used in the present study have been described (14). After washing twice with PBBS containing 2% FBS, bound IgM and IgG were differentially detected by incubating the cells either with FITC-conjugated anti-mouse IgM (µ-chain specific, Southern Biotechnology Associates, Inc., Birmingham, AL, USA) at 5 µg per 10^6 cells or with FITC-conjugated anti-mouse IgG (γ-chain specific, Zymed Laboratories, Inc., South San Francisco, CA, USA) at 1.5 µg per 10^6 cells, respectively, for 20 min. Stained cells were washed three times before being examined by flow cytometry as described above.

Purification of T cells and their transfer

Purification of T cell subsets from the spleen of naive, immunized and/or FV-infected mice was performed by using mAb-conjugated magnetic microbeads and a magnetic cell sorter I (Miltenyi Biotec GmbH, Bergisch Gladbach, Germany) according to the manufacturer's instructions. Spleen cells were first treated with Tris-buffered ammonium chloride solution to lyse erythrocytes, and incubated with anti-B220 mAb-conjugated magnetic beads to remove B cells by passing through a negatively selecting CS column. To purify $CD4^+$ T cells, $B220^-$ cells were then incubated with anti-CD8 mAb-conjugated magnetic beads, passed through a CS column to remove $CD8^+$ cells and then incubated with anti-CD4 mAb-conjugated microbeads to positively select $CD4^+$ cells by passing through a VS column. Multicolor flow cytometric analyses revealed that the resultant cell preparation was >99% $CD4^+$. $CD8^+$ cells were similarly purified from $B200^-$ cells by removing $CD4^+$ cells and positively selecting $CD8^+$ cells. This preparation was 97–98% $CD8^+$ in repeated experiments. Percentages of $CD4^+$ and $CD8^+$ T cells in the spleen after FV inoculation were determined by flow cytometry in $CB6F_1$ mice immunized with peptide i. To reconstitute the full number of T cells that belonged to each subset in the immunized mice, unimmunized recipient mice were injected intravenously with 2×10^7 to 2.5×10^7 $CD4^+$ or $CD8^+$ T cells per mouse.

Depletion of $CD4^+$ T cells

Anti-mouse CD4 mAbs were purified from culture supernatant of the hybridoma cell GK 1.5 (29) as described previously (13, 25). Control rat myeloma IgG was purchased from Zymed Laboratories, Inc. The amount of the mAbs required for complete depletion of $CD4^+$ T cells from $CB6F_1$ mice was determined by intravenously administering the purified mAb and monitoring the number of $CD4^+$ and $CD8^+$ cells in the spleen by flow cytometry. The schedule of mAb administration finally adopted was as follows: $CB6F_1$ mice were immunized with 3 µg per mouse of peptide i emulsified in CFA. Three weeks later, mice were intravenously given 125 µg per mouse purified anti-CD4 mAb. Five additional intravenous doses of 125 µg per mouse anti-CD4 mAb were given 2, 4, 6, 9 and 18 days after the first administration. The negative-control rat IgG was given to a separate group of mice on the same schedule. Mice were inoculated with 150 spleen focus-forming units (SFFU) FV 7 days after the beginning of the mAb administration. Peripheral blood was collected from three representative animals at each time point through the tail vein at post-infection day (PID) 3, 6, 10 and 13, and flow cytometric analyses were performed to confirm the absence of $CD4^+$ T cells.

Statistical analyses

Differences in survival curves expressed by the Kaplan–Meier method were compared by a Mantel–Haenszel logrank test using GraphPad Prism 3 (GraphPad Software, Inc., San Diego, CA, USA). The numbers of mice that developed or lacked splenomegaly were compared between the immunized and unimmunized groups by Fisher's exact test. Average numbers of infectious centers between experimental groups and anti-leukemia cell antibody titers were compared by Mann–Whitney's *U*-test because these values were not expected to follow a Gaussian distribution. Differences in IgM and IgG titers of virus-neutralizing antibodies were compared by paired *t*-test. Spleen weights and percentages of $TER\text{-}119^+$, $gp70^+$ cells in the spleen and bone marrow between the immunized and unimmunized groups of mice were compared by Student's or Welch's *t*-test depending on whether the variances of the compared samples were estimated to be equal or not.

Results

Suppression of the early growth of FV-infected erythroid cells and prevention of leukemic death in highly susceptible $CB6F_1$ mice by immunization with a single-epitope $CD4^+$ T cell vaccine

Mice of BALB/c background are extremely susceptible to FV-induced disease, and $CB6F_1$ mice all died within 60 days after infection with only 15 SFFU of FV without showing any signs of spontaneous recovery (Fig. 1a). This was striking because even (B10.A × A/WySn)F_1 mice that have been used as a strain typically susceptible to FV infection have shown mortality rates of 70–80% at 90–100 days after inoculation with 15 SFFU FV (1, 5). Therefore, the following immune protection experiments were performed in $CB6F_1$ mice with 150 SFFU of FV to ensure that peptide-induced immune responses protect this highly susceptible strain of mice from doses of FV large enough to kill all unimmunized animals.

The efficacy of peptide i in priming $CD4^+$ T cells *in vivo* has been demonstrated by the establishment of $CD4^+$ T cell clones reactive to this peptide from the peptide-immunized $CB6F_1$ mice (23), and by more pronounced expansion of $CD4^+$ T cells in the spleen after FV challenge in the peptide-immunized than in the unimmunized control $CB6F_1$ mice (14). To directly demonstrate the priming of $CD4^+$ T cells in peptide-immunized

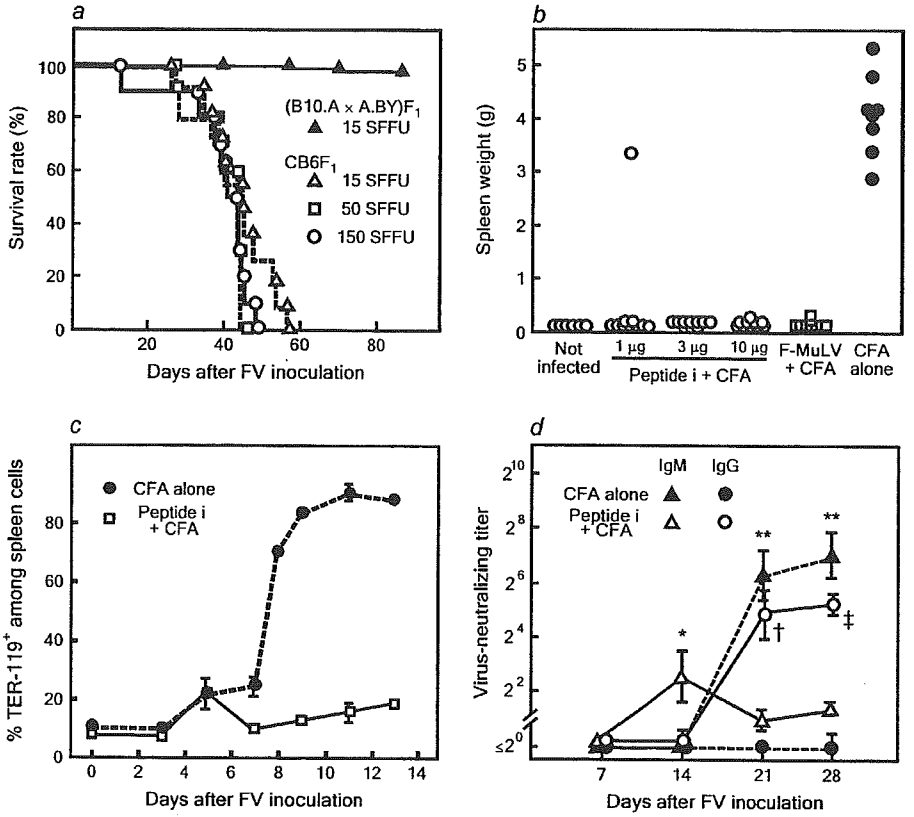

Fig. 1. Development of FV-induced disease in $CB6F_1$ mice and its prevention by immunization with the single-epitope peptide i. (a) $CB6F_1$ mice were inoculated intravenously with 15 ($n = 11$), 50 ($n = 10$) or 150 SFFU ($n = 10$) of FV and the survival of infected animals was examined. Similar curves were obtained in three repeated experiments. For a comparison, $(B10.A \times A.BY)F_1$ ($n = 40$) mice were also infected with 15 SFFU of FV and followed for their survival until PID 90. (b) The effect of different doses of peptide i on protective immunity against FV. $CB6F_1$ mice were immunized once with 1, 3 or 10 µg per mouse of peptide i in CFA, or given a CFA emulsion of purified F-MuLV particles at 40 µg per mouse. The F-MuLV particles used had been inactivated by UV irradiation as described (19). Control mice were given CFA without any peptide (CFA alone). Mice were challenged with 150 SFFU FV 4 weeks after immunization, and their spleen weight was measured as soon as they died (CFA alone group) or were killed at PID 45. Significant differences in spleen weights were only observed between the CFA alone group and five other groups ($P < 0.006$). (c) Changes in the percentages of TER-119^+ erythroid cells among nucleated spleen cells of FV-infected $CB6F_1$ mice. Mice were immunized once with 10 µg (5 nmol) of peptide i in CFA or given CFA alone and inoculated with FV 4 weeks later. Each data point shows mean ± SEM calculated by using four to five individual mice per group. (d) Changes in serum titers of virus-neutralizing IgM and IgG antibodies after FV infection. $CB6F_1$ mice were either immunized once with 10 µg per mouse peptide i in CFA or given CFA alone, and challenged with 150 SFFU FV 4 weeks later. Each data point shows mean ± SEM calculated by using seven to eight individual mice per group. Serum titers of F-MuLV-neutralizing IgM and IgG were compared by paired *t*-test: *IgM titers are significantly higher than IgG titers at $P < 0.05$; **$P < 0.0001$. †, IgG titers are significantly higher than IgM titers at $P < 0.05$; ‡, $P < 0.01$.

$CB6F_1$ mice, $CD4^+$ and $CD8^+$ T cells were purified from $CB6F_1$ mice at 3 weeks after a single immunization with peptide i, and re-stimulated *in vitro* in the presence of syngeneic, γ-irradiated spleen cells as antigen-presenting cells (APCs). As shown in Fig. 2(a), $CD4^+$ T cells purified from the immunized $CB6F_1$ mice proliferated vigorously when stimulated with 1 µM of peptide i, while the proliferative responses of $CD4^+$ T cells purified from the control mice given CFA alone were below the background level even when stimulated with 20 µM of the same peptide. As controls, $CD8^+$ T cells purified either from the peptide-immunized or unimmunized control mice showed no significant proliferative responses even when stimulated with 20 µM peptide i.

To determine the minimal amount of the peptide that is required for the effective induction of protective immunity against FV infection, three different amounts of peptide i were given as a single intradermal immunization to $CB6F_1$ mice, and immunized mice were challenged with 150 SFFU FV. Since most of the unimmunized $CB6F_1$ mice died by PID 45 (Fig. 1a), infected mice were either dissected soon after their death or killed at PID 45, and their spleen weight was measured. As shown in Fig. 1(b), a single immunization with 3 µg (1.7 nmol) per mouse of peptide i was as effective as 10 µg per mouse of the same peptide, and only one mouse among the ten that were given 1 µg peptide i developed splenomegaly after FV infection. Thus, in the following experiments, 3–10 µg per mouse of peptide i was used as a sufficiently large protective dose.

FV-induced early splenomegaly is caused by the rapid growth and differentiation of SFFV-infected erythroid progenitor

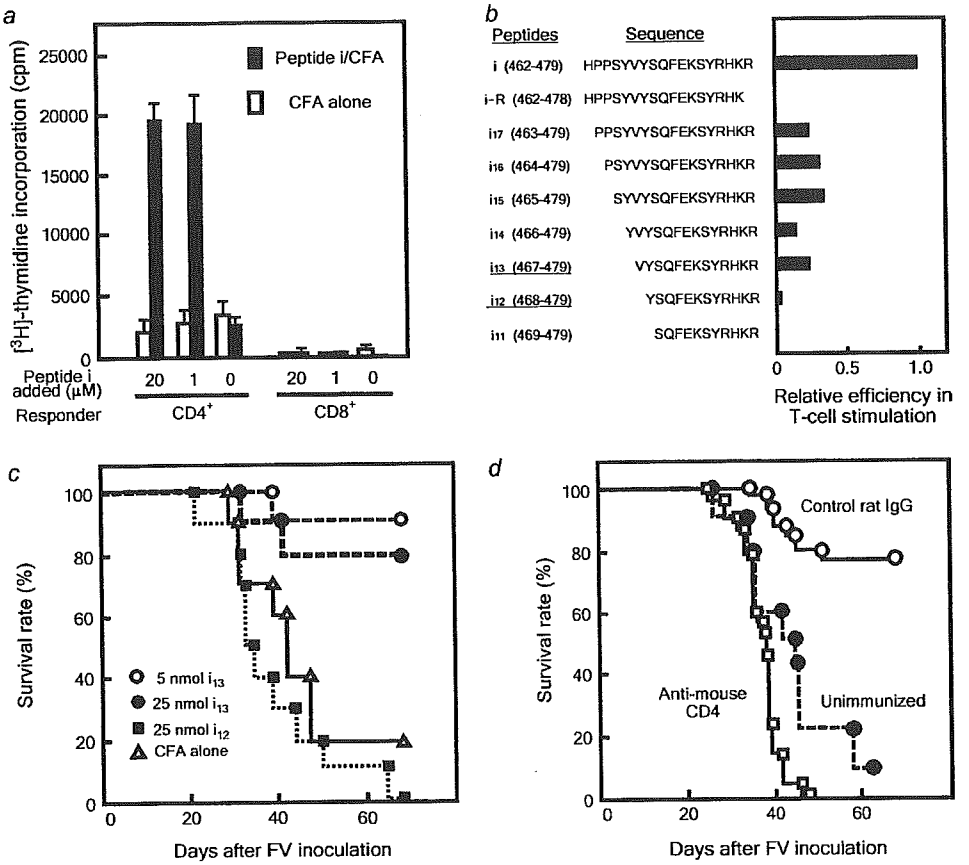

Fig. 2. Priming of CD4⁺ T cells by peptide immunization and efficacies in CD4⁺ T cell stimulation *in vitro* and immune protection *in vivo* of peptide i and its truncated derivatives. (a) Both CD4⁺ and CD8⁺ T cells were purified from the spleen of $CB6F_1$ mice at 3 weeks after a single immunization with 10 μg per mouse peptide i emulsified in CFA. Proliferative responses were measured 2 days after stimulation with the indicated concentration of peptide i along with syngeneic, γ-irradiated spleen cells as APCs. CD4⁺ and CD8⁺ T cells purified from $CB6F_1$ mice given CFA without a peptide (CFA alone) were used as controls. Data shown are averages + SEM of triplicate cultures, and the experiments were performed three times with essentially the same results. (b) Sequences of peptide i and its truncated derivatives, and their relative efficiency to stimulate FV-specific T cell clones. Representative data obtained with clone F5-5 are shown, while the data obtained with clone FP7-11 were consistent with those presented here. ED_{50} of the full-length i was 0.2 μM. (c) Protection of $CB6F_1$ mice against FV infection with the truncated peptide. $CB6F_1$ mice ($n = 10$ per group) were immunized once with 5 nmol per mouse of peptide i_{13}, 25 nmol per mouse of i_{13} or 25 nmol per mouse of i_{12}. Control mice were given CFA emulsion containing no peptide. Four weeks later, they were inoculated with 150 SFFU FV and followed for their survival. (d) $CB6F_1$ mice ($n = 22$ per group) were immunized once with 3 μg per mouse of peptide i and repeatedly injected with the anti-CD4 mAb (□) or control rat IgG (○). Four weeks after immunization, these mice and a group of unimmunized control mice (●) were inoculated with 150 SFFU FV and followed for their survival.

cells, and the resultant erythroblasts and maturing red cells are marked by mAb TER-119 (27). Thus, bursting of the TER-119⁺ erythroid cells was observed in the unimmunized control mice starting from PID 7, following the slow initial increase of the same cell population (Fig. 1c). On the other hand, the number of TER-119⁺ erythroid cells in the spleen started to decrease between PID 5 and 7 in the $CB6F_1$ mice that had been immunized once with peptide i. Virus-neutralizing antibodies in the serum were not detectable at PID 7 in FV-infected $CB6F_1$ mice regardless of whether they had been immunized with peptide i or not (Fig. 1d). In the $CB6F_1$ mice immunized with peptide i, virus-neutralizing IgM became detectable by PID 14, and the antibodies switched to IgG between PID 14 and 21. In the unimmunized mice, however, virus-neutralizing antibodies became detectable at PID 21, a week later than in the peptide-immunized mice, and they did not switch to IgG even at PID 28. These results indicated that the FV-induced expansion of erythroid cells was prevented in the peptide-immunized mice before virus-neutralizing antibodies became detectable in the serum.

Protection against FV disease correlates with CD4⁺ T cell stimulation

To identify the minimal effective sequence of the peptide vaccine, a series of truncated peptides were compared for their *in vitro* T cell-stimulating and *in vivo* protection efficacies (Fig. 2b and c). It was clear that the C-terminal Arg residue was indispensable for the recognition of this epitope by T cells. In fact, a 17-mer peptide, i-R, that lacked only the C-terminal

Arg totally lost the ability to stimulate $CD4^+$ T cell proliferation *in vitro*, while another 17-mer, i_{17}, that retained the Arg residue but lacked the N-terminal His kept the ability, albeit less efficiently than peptide i, to stimulate the T cells. When N-terminal residues were further removed from the 18-mer i and their efficacy to stimulate the $CD4^+$ T cells was examined through the range of concentrations between 0.01 and 20 μM, the 13-mer (i_{13}) retained the T cell-stimulating activity and showed a stimulatory effect comparable to peptide i_{17}, while the 12-mer (i_{12}) showed a stimulatory effect <1/24 of that of the full-length peptide i. Peptide i_{11} did not induce significant proliferation even when as much as 20 μM was added to the culture. In line with this result, the 13-mer retained the ability to induce protection against FV challenge in immunized $CB6F_1$ mice, while the 12-mer did not protect the same strain of mice against FV-induced disease even when five times more molecules were administered (Fig. 2c).

The requirement of $CD4^+$ T cells for the peptide-induced immune protection was further confirmed by depleting $CD4^+$ T cells from vaccinated $CB6F_1$ mice. The adopted schedule of the antibody administration resulted in undetectable $CD4^+$ T cells in the spleen in separately examined uninfected animals for a period equivalent to PID 0–14, and lack of $CD4^+$ T cells in the peripheral blood was confirmed in the vaccinated and infected group on PID 3–13 (data not shown). Antibody-induced depletion of $CD4^+$ T cells abrogated the efficacy of peptide immunization, and $CD4^+$ T cell-depleted animals died even more rapidly than the unimmunized control mice ($P < 0.05$). Injection of the control rat IgG did not affect the protective efficacy of the peptide vaccine, and ~80% of the peptide-immunized $CB6F_1$ mice that had been given the control antibody survived past PID 60 (Fig. 2d).

Peptide-induced immune protection against FV-induced disease in $CB6F_1$ mice genetically lacking a single component of the immune system

To examine possible effectiveness of the peptide immunization in mice genetically lacking either $CD8^+$ T or B cell components of the immune system, we produced $CB6F_1$ mice with a homozygous disruption of the $\beta_2 m$ gene or of the Ig μ-chain gene. The absence of $CD8^+$ T or B lymphocytes, respectively, was confirmed by flow cytometric analyses of the spleen and PBMCs (data not shown). In accordance with the prior experiments (Figs 1 and 2), ⩾80% of the wild-type $CB6F_1$ mice were protected against FV infection when immunized with peptide i. Protective efficacy of the 13-mer peptide, i_{13}, was further confirmed, and the development of early splenomegaly was prevented in 70% of the $CB6F_1$ mice given i_{13} (Fig. 3a). Surprisingly, when $CB6F_1$-$\beta_2 m^{-/-}$ mice lacking $CD8^+$ T cells were immunized with peptide i, only <30% of the immunized mice developed splenomegaly and >70% survived until PID 100 in repeated experiments (Fig. 3). The observed survival curves were not significantly different between the peptide-immunized wild-type and $\beta_2 m^{-/-}$ groups ($P > 0.4$), indicating a similar effectiveness of the peptide vaccine both in the presence and absence of $CD8^+$ T cells. On the other hand, when the mice of the same susceptible $CB6F_1$ background that lacked B cells due to the homozygous *μMT* mutation were immunized with peptide i, they developed splenomegaly and all died by PID 100, indicating crucial roles of B cells for the peptide-induced immune protection. Interestingly, however, the temporal changes in the incidences of splenomegaly and leukemic death delayed significantly in repeated experiments in the peptide-immunized, B cell-deficient mice compared with those in the unimmunized control mice of the same deficiency (Fig. 3c and f). The delay in the development of splenomegaly in the peptide-immunized *μMT/μMT* mice was also substantiated by flow cytometric enumerations of FV-infected erythroid cells: at PID 7, 28.2 ± 3.7% ($n = 5$) of the nucleated spleen cells were positive for both TER-119 and F-MuLV gp70 in the unimmunized control mice, while the proportion of the TER-119^+, $gp70^+$ cells in the spleen was significantly smaller ($P < 0.05$) 12.1 ± 8.2% ($n = 5$) in the peptide-immunized *μMT/μMT* mice. The effect of peptide immunization was more striking in the bone marrow where the percentage of TER-119^+, $gp70^+$ cells in the unimmunized mice was 11.1 ± 4.4%, while that of the peptide-immunized mice was 0.72 ± 0.22% ($P < 0.03$) at PID 7. These results indicate some functions of non-B cells in delaying the FV-induced disease development.

Elimination of FV-producing cells from the spleen and bone marrow in the $\beta_2 m^{-/-}$ mice immunized with peptide i

We next compared the numbers of FV-infected cells between peptide-immunized and unimmunized control mice using infectious center assays. The relative ratio in the number of FV-producing cells in the spleen between the peptide-immunized and unimmunized mice started to decrease at PID 8 as observed in the previous experiments (13, 14), and FV infectious centers became undetectable by our assays by PID 28 in peptide-immunized wild-type mice (Fig. 4a). The lack of detectable FV-producing cells in the spleen of all the tested, peptide-immunized $CB6F_1$ mice was confirmed by seeding the cells prepared from the entire spleen ($>10^8$) of each animal as infectious centers at PID 28. The number of FV-producing cells in the bone marrow was also significantly lower in the peptide-immunized wild-type mice than in the unimmunized control mice at PID 8, 14 and 21, and became undetectable at PID 28 (Fig. 4d). At PID 28, 2.1×10^7 bone marrow cells were tested from each mouse and no infectious centers were detectable by our assays in any of the examined animals. In the $CB6F_1$-$\beta_2 m^{-/-}$ mice, the numbers of FV-producing cells in the spleen and bone marrow were significantly lower in the peptide-immunized than in unimmunized control mice at PID 14 and 28 (Fig. 4b and e), in accordance with the observed effectiveness of the peptide immunization in preventing the FV-induced disease development in the absence of $CD8^+$ T cells (Fig. 3). It should be noted that in seven of the nine immunized animals tested at PID 28 no infectious centers were detectable even when the cells of the entire spleen were inoculated into the culture. However, there were also individuals among the peptide-immunized $\beta_2 m^{-/-}$ mice in which FV-producing cells were still detectable in the spleen or bone marrow at PID 28 (Fig. 4b and e), while such cells were not detectable in any of the immunized wild-type mice tested at the same time point. These results imply that $CD8^+$ T cells were not necessarily required but may play some roles in the elimination of virus-infected cells in peptide-immunized $CB6F_1$ mice.

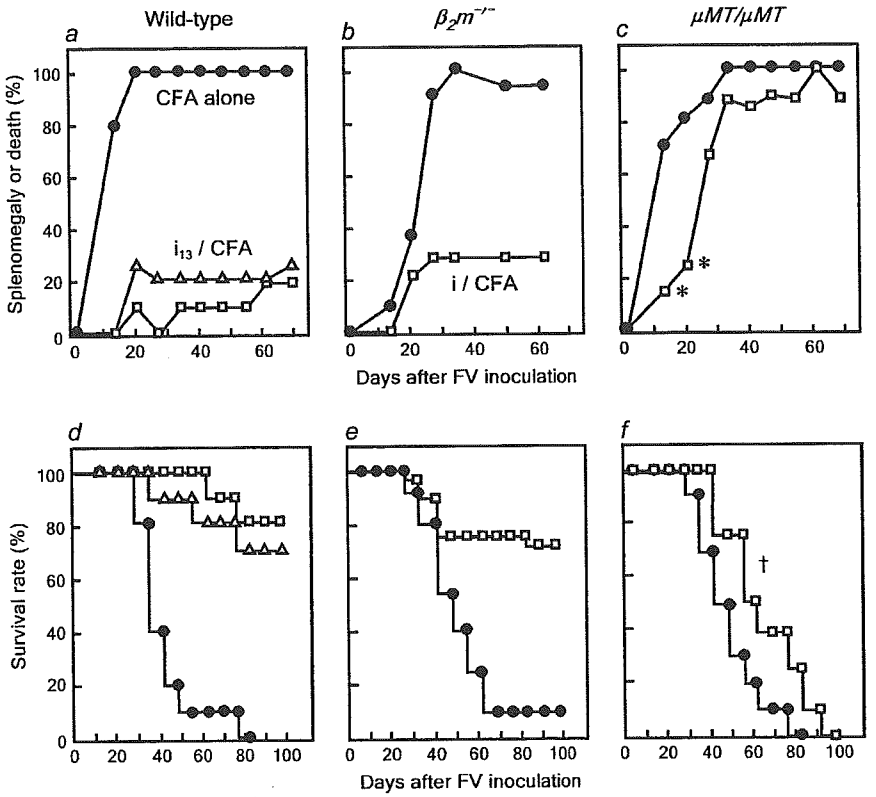

Fig. 3. Effects of immunization with peptide i on the development of FV-induced disease in $CB6F_1$ mice lacking $CD8^+$ T or B cells. Wild-type $CB6F_1$ mice (a and d), $CB6F_1$ mice lacking $CD8^+$ T cells due to homozygous targeting of the $\beta_2 m$ gene (b and e) and $CB6F_1$ mice lacking B cells due to homozygous targeting of the membrane exon of Ig μ-chain gene (c and f) were either immunized with 10 μg per mouse of peptide i in CFA (□) or given CFA alone (●). Another group of the wild-type mice were immunized with 10 μg per mouse of peptide i_{13} in CFA (Δ). Four weeks later, they were inoculated with 150 SFFV FV and followed for the development of splenomegaly and leukemic death. In (c), * indicates significant differences in the frequency of splenomegaly between the immunized and control groups ($P < 0.001$), and in (f), † indicates significant difference between the two survival curves ($P = 0.041$). The number of animals in each group were: (a) and (d), □, 10; Δ, 10; ●, 10; (b) and (e), □, 23; ●, 20 and (c) and (f), □, 12; ●, 16. The experiments were performed twice with essentially identical results.

In accordance with the lack of protection against FV-induced disease development, virus-producing cells constantly increased between PID 5 and 21 in the spleen and bone marrow of the $CB6F_1$-*μMT/μMT* mice, regardless of whether the hosts were immunized with peptide i or not. Interestingly, however, the numbers of virus-producing cells both in the spleen and bone marrow were significantly lower in the peptide-immunized, B cell-deficient mice than those in the unimmunized control mice of the same deficiency at PID 8 (Fig. 4f). This observation is consistent with the significant delay in the development of early splenomegaly and leukemic death (Fig. 3), and smaller numbers of TER-119^+ and viral $gp70^+$ FV-infected erythroid cells in the spleen and bone marrow in peptide-immunized, B cell-deficient $CB6F_1$ mice.

Priming and re-activation of $CD4^+$ T cells in the peptide-immunized μMT/μMT mice

To examine the possibility that the observed inefficiency in anti-FV protection of the immunization with peptide i in $CB6F_1$-*μMT/μMT* mice might be due to the lack of APC activity, rather than antibody-producing function, of B lymphocytes, peptide-specific proliferative responses were compared between the wild-type and *μMT/μMT* animals. When $CD4^+$ T cells purified from the wild-type $CB6F_1$ mice previously immunized with peptide i were used as responders, irradiated spleen cells both from the wild-type and from the *μMT/μMT* animals induced strong proliferative responses, although the peptide-specific proliferation was significantly weaker when *μMT/μMT* instead of the wild-type spleen cells were used as APC (Fig. 5a). FV infection significantly affected the APC function of wild-type spleen cells, but that of *μMT/μMT* spleen cells was not significantly reduced when used at PID 10. Similar results were observed when $CD4^+$ T cells purified from immunized *μMT/μMT* animals were used as responders. Thus, $CD4^+$ T cells were primed with peptide i in the absence of B cells, and spleen cells from *μMT/μMT* animals could present the peptide antigen to primed $CD4^+$ T cells, albeit less efficiently than the wild-type spleen cells, even after FV infection. Successful priming of $CD4^+$ T cells and their re-activation upon FV infection in *μMT/μMT* animals were further confirmed *in vivo* by analyzing the expression of an early activation marker, CD69, on T cells. Upon FV infection of peptide-immunized $CB6F_1$-*μMT/μMT*

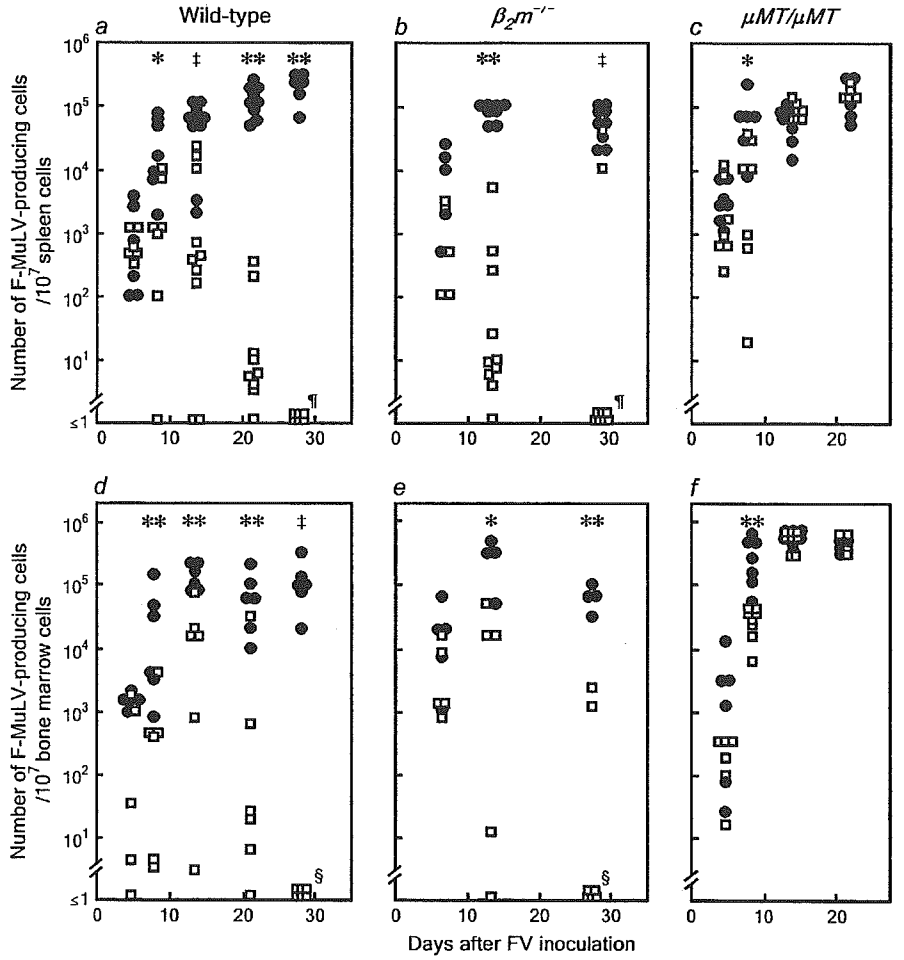

Fig. 4. Effects of immunization with peptide i on the number of FV-producing cells in $CB6F_1$ mice lacking $CD8^+$ T or B cells. Wild-type $CB6F_1$ mice (a and d), the $CB6F_1$ mice lacking $CD8^+$ T cells (b and e) and the $CB6F_1$ mice lacking B cells (c and f) were either immunized with 10 μg per mouse of peptide i in CFA (□) or given CFA alone (●). Four weeks later, they were inoculated with 150 SFFV FV and FV-producing infectious centers were enumerated in the spleen (a–c) and bone marrow (d–f). Each data point shows the actual number of infectious centers detected from each individual mouse. At least 10^7 spleen and bone marrow cells were tested from each animal. At PID 28, the cells prepared from the entire spleen ($>10^8$, ¶) and 2.1×10^7 (from wild-type mice) or 3.1×10^7 (from $\beta_2m^{-/-}$ mice) bone marrow cells (§) were inoculated as infectious centers to ensure the lack of detectable virus-producing cells. Infectious centers were undetectable from any of the tested animals indicated with ¶ or § at PID 28. Statistical significance of the difference between the immunized and unimmunized groups at each time point was examined: $*P < 0.04$; $**0.001 < P < 0.01$; ‡, $0.0002 < P < 0.001$.

mice, an increase in the proportion of $CD69^+$ cells among $CD4^+$ T cells was readily detectable (Fig. 5b). The percentages of $CD69^+$ cells among $CD4^+$ T cells in the spleen at PID 7 were significantly higher in the peptide-immunized than in the unimmunized animals, indicating re-activation of peptide-primed T cells upon FV infection (Fig. 5c). The effect of peptide immunization on the induction of CD69 expression was even more pronounced when bone marrow cells were tested (Fig. 5d). Interestingly, the $CD69^+$ population among $CD8^+$ T cells also showed a significant increase when peptide-immunized and unimmunized *μMT/μMT* mice were compared at PID 7, confirming the previously demonstrated activation of $CD8^+$ cytotoxic cells at PID 7 (14).

Production and class switching of serum antibodies reactive to the surface of FV-induced leukemia cells in the peptide-immunized mice

Although virus-neutralizing antibodies were not detectable in FV-infected animals until PID 14 (Fig. 1d), non-neutralizing anti-FV antibodies might have been produced at earlier time points, and might have contributed to the observed decrease in the number of FV-infected cells in the vaccinated animals, which was evident at as early as PID 7 (Figs 1c and 4). Thus, the possible presence of anti-FV antibody in the serum was examined using FV-induced leukemia cells as indicators. The hemisyngeneic ($H2^{b/b}$), FV-induced leukemia cells Y57-2C expressed both the F-MuLV *gag* and *env* gene products as

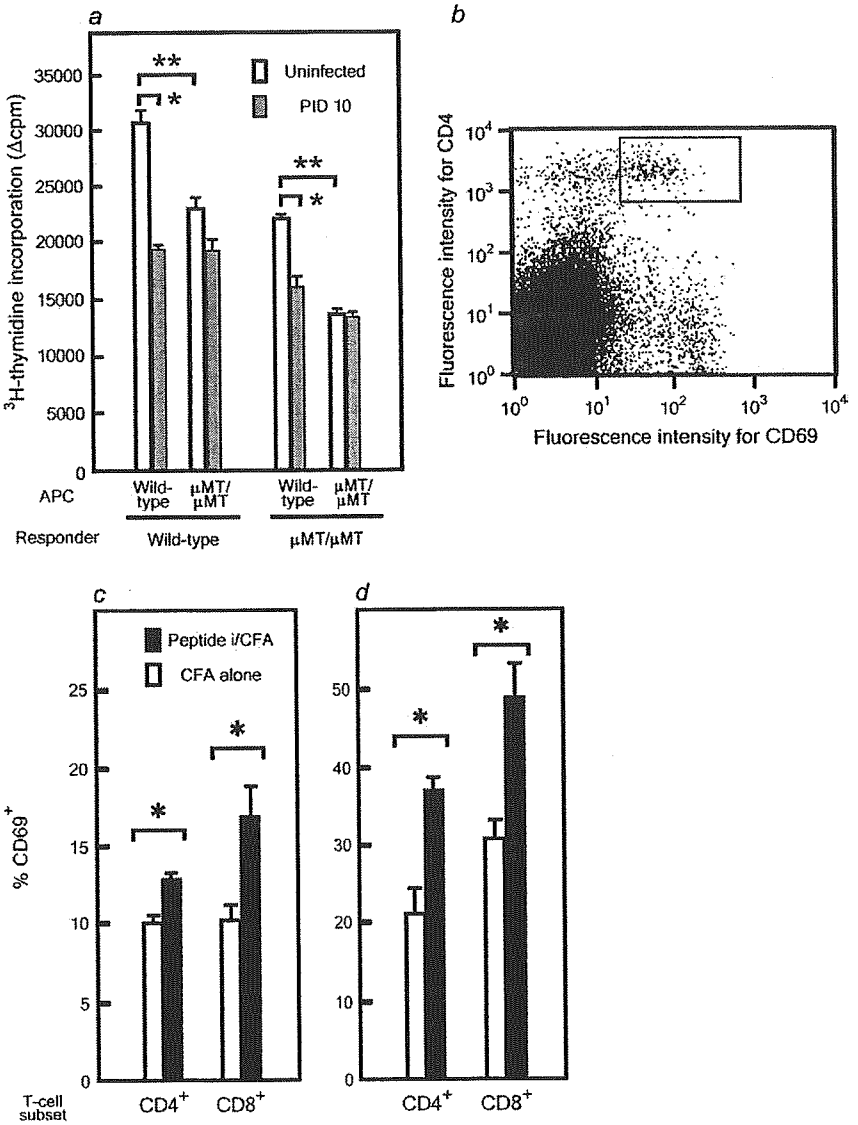

Fig. 5. Priming and re-activation of CD4$^+$ T cells with peptide i in the B cell-deficient mice. (a) CD4$^+$ T cells were purified from the spleen of wild-type and homozygous *μMT/μMT* CB6F$_1$ mice at 3 weeks after a single immunization with 10 μg per mouse peptide i emulsified in CFA. Proliferative responses were measured at 2 days after stimulation with 1 μM peptide i along with the indicated APC. Spleen cells as APC were prepared from the wild-type and *μMT/μMT* CB6F$_1$ mice either without FV inoculation or at PID 10, and γ-irradiated. The magnitude of antigen-specific proliferation is shown by Δ counts per minute (c.p.m.) in this chart by subtracting the average [^{3}H]thymidine ([^{3}H]TdR) incorporation into the cultures containing no peptide from that in the peptide-containing cultures. Levels of [^{3}H]TdR incorporation into the cultures without a peptide were <120 c.p.m. Data shown are averages + SEM of triplicate cultures, and the experiments were performed twice with essentially the same results. *, significantly different at $P < 0.01$; **$P < 0.001$. (b) A representative pattern of CD69 expression on CD4$^+$ T cells in the bone marrow of the *μMT/μMT* mice previously immunized with peptide i. The small rectangle indicates the gate used to calculate the percentage of CD69$^+$ cells among CD4$^+$ T cells. (c) and (d) Comparison of the percentages of CD69$^+$ activated cells among CD4$^+$ and CD8$^+$ T cells in the spleen (c) and bone marrow (d) at 7 days after FV inoculation between the peptide-immunized and unimmunized *μMT/μMT* mice. Data are averages + SEM calculated with five mice per group. *, the percentage of CD69$^+$ population is significantly higher in the immunized than in the unimmunized mice at $P < 0.005$.

well as SFFV gp55 on their surfaces (Fig. 6a). Sera from FV-infected CB6F$_1$ mice bound onto the surface of Y57-2C cells, and geometric means of the fluorescence intensities decreased in proportion to serum dilutions (Fig. 6b). Therefore, at each time point titers of serum antibodies reactive to the surface of the FV-induced leukemia cells, designated hereinafter anti-leukemia cell antibody titers, were determined by dividing geometric means of fluorescence intensities obtained by incubating the indicator cells with a 1/16 dilution of serum samples by the geometric mean of fluorescence intensities obtained with the same dilution of pooled control serum collected from uninfected CB6F$_1$ mice. Interestingly,